PFC/JA-83-4

A FAST NEUTRON SPECTROMETER FOR D-D FUSION NEUTRON MEASUREMENTS AT THE ALCATOR C TOKAMAK

W. A. Fisher, S. H. Chen, D. Gwinn, R. R. Parker

Plasma Fusion Center
Massachusetts Institute of Technology
Cambridge, MA 02139

May 1983

This work was supported by the U.S. Department of Energy Contract No. DE-AC02-78ET51013. Reproduction, translation, publication, use and disposal, in whole or in part by or for the United States government is permitted.

A Fast Neutron Spectrometer for D-D Fusion Neutron Measurements at the Alcator C Tokamak

W. A. Fisher* and S. H. Chen

Nuclear Engineering Department
Massachusetts Institute of Technology
Cambridge, MA 02139

and

D. Gwinn and R. R. Parker

Plasma Fusion Center
Massachusetts Institute of Technology
Cambridge, MA 02139

Abstract

A neutron spectrometer using a high pressure ^{3}He ionization chamber has been designed and used to measure the neutron spectrum from an ohmically heated deuterium plasma. The resolution of the spectrometer at 2.45 MeV is determine to be 46 keV full width at the half maximum (FWHM). Particular attention has been paid to optimizing the detector shielding and collimation to reject thermal and epithermal neutrons scattered from the tokamak structure. As a result, measurements indicate that the ratio of the number of counts in the 2.45 MeV peak to the total number of detected neutron events is 1/67. For the 8 μsec amplifier time constant used, a count rate as high as 44 counts per second has been achieved in the thermonuclear peak. The observed spectra have been compared with calculated spectra using the MCNP Monte Carlo Neutral Particle Transport code and they show good agreement. There is little evidence of neutrons produced from photoneutron reactions or electrodisintegration. It has been possible to confirm that the shape of the thermonuclear peak is consistent with the Gaussian shape predicted and that the ion temperature as determined from the line width is consistent with other Alcator C ion temperature diagnostics, and follows the trends predicted by the theory of Doppler line broadening.

*Present Address: National Nuclear Corp.
1904 Colony St.
Mountain View, CA 94043

I. Introduction

The fact that the fusion neutron spectrum could be used to study the ion energy distribution of a thermonuclear plasma has been known since the early days of fusion research. In 1967 Lehner and Pohl [1] presented a paper in which most of the theory used today was detailed. Unfortunately, very little use has been made of this knowledge because of the difficulty in making high resolution measurements of fusion neutrons. The work discussed here represents a successful attempt at such a measurement.

Strachan et al. [2] have used a ^{3}He ionization chamber at the Princeton Large Torus (PLT) to measure the neutron spectrum due to a beam heated plasma, but were unable to resolve the D-D fusion peak for an ohmically heated plasma [3]. The measurement has been possible at Alcator C because the plasma density is an order of magnitude greater than PLT, resulting in a ratio of fusion neutrons to non-fusion neutrons which is two orders of magnitude better than PLT. In addition, we have improved the ion chamber shielding and collimation obtaining a lower thermal to fast neutron count ratio, thus achieving a much improved count rate performance at the D-D peak. The emphasis of this paper is on the design of the spectrometer. Additional details on the measurements at Alcator C may be found in reference [4].

The Alcator C fusion device is a high field compact tokamak located at and operated by the Massachusetts Institute of Technology for the U.S.

Department of Energy. Figure 1 shows a diagram of the machine. The design parameters for the machine are displayed in table 1.

An important result of a neutron spectrum measurement is that it is possible to identify the physical process which generated the neutron from its energy. Five processes are known to be sources of neutrons in an Alcator C deuterium plasma discharge: photoneutron reactions, electrodisintegration of deuterium, photodisintegration of deuterium, thermonuclear fusion of deuterium, and fusion of deuterium and tritium. These processes have been described in detail in references [3] and [5]. Photoneutron production, and photodisintegration of deuterium are processes which occur at the ring of molybdenum blocks used to define the plasma discharge (limiter). Electrodisintegration is a volume process but has a cross-section which is several orders of magnitude smaller than the D-D cross-section for the particle energies expected in Alcator C plasmas. All the processes except the thermonuclear D-D and D-T reactions are a result of supra-thermal electrons which are produced for some plasma conditions [6]. It is possible to limit the production of these 'run-away electrons' by controlling the plasma discharge conditions.

Tritium produced in the D(d,p)T reaction can also react via D-T reaction to produce 14.7 MeV neutrons. These neutrons would be expected to cause a background of neutrons above the D-D peak due to down-scattering in the room and machine structure. Chrien [7] has measured the D-T rate to D-D rate ratio for PLT and found it to be between 10^{-3} and 10^{-4}.

Figure 2 shows how each of the processes might affect a neutron spectrum. This figure is based mainly on a spectrum measured by Stra-

chan and Jassby [3] using a ^{3}He ionization of the same design as used here for an ohmic discharge at the Princton Large Torus PLT. Their results were obtained at a plasma density roughly an order of magnitude lower than that used here where non-thermonuclear processes are important. As will be seen later, thermonuclear D-D reactions dominated the neutron spectra measured here.

The D-D thermonuclear neutron rate is given by

$$R = \frac{n^2}{2} \iint f(\underline{v}_1)\, f(\underline{v}_2)\, |\underline{v}_{rel}|\, \sigma(\underline{v}_{rel})\, d^3v_1\, d^3v_2 \qquad (1)$$

where n is the Deuterium density, $f(\underline{v}_1)$,$f(\underline{v}_2)$ are the distribution functions of the reacting D-D pair, $\underline{v}_{rel}$ is the relative velocity, $\underline{v}_1\underline{v}_2$, and $\sigma(v_{rel})$ the nuclear cross-section. A general form for the neutron spectrum can be obtained by applying the condition that the neutron have an energy $\frac{3}{4}(Q+E_{rel})$ in the center of mass coordinate system. A general formulation is given in Lehner [8]. However, the result of evaluations of the spectrum for the case of the isotropic Maxwellian ion distribution function is used here [8,9,10,11]. Williams [10], for example, found that the three-dimensional isotropic Maxwellian ion velocity distribution, the expected distribution for Alcator C plasmas, would produce an approximately, Gaussian energy spectrum with a mean energy given by

$$\langle E_n \rangle = \frac{3}{4}\left[Q + \frac{kT}{2} + \left(\frac{bkT}{2}\right)^{2/3} \right] \qquad (2)$$

and the line width FWHM in keV is given by

$$\Delta E_n = 82.5\sqrt{kT} \tag{3}$$

where kT is the plasma temperature in keV as defined by the Maxwellian distribution. In equation (2), b is the coefficient in the Gamow cross-section,

$$\sigma(E_{rel}) = \frac{E_o\ \sigma(E_o)}{E_{rel}}\ e^{-b/\sqrt{E_{rel}}} \tag{4}$$

where E_o is an energy at which the cross-section is known.

Equation (3) gives the line width for a spatial and time invariant plasma source. In a real measurement the line width will represent the average over space and time of the plasma distribution. However, ion temperature representing the maximum ion temperature in both space and time is a more characteristic plasma parameter and is generally used. Thus a correction has to be made to obtain the peak central ion temperature from the temperature measured from the line width of the neutron spectrum.

As will be seen in section IV it is necessary to integrate over a large portion of an Alcator plasma and also to sum the spectra of many plasma discharges (shots) together to obtain sufficient statistics in the neutron spectrum. Figure 3 illustrates a typical plasma discharge. The shaded area represents the time during which the neutron spectrum was collected during the discharge. The ion temperature can be deduced from the total neutron rate measurement and is estimated to vary by about 11% over the shaded region. However, the effect of averaging the

ion temperature from a measurement of the peak width is calculated to yield a temperature which is 0.96 the peak ion temperature or a 4% correction.

The ion temperature in Alcator C is assumed to be poloidally and toroidally constant but to vary with the minor radius as given by

$$T_i(r) = T_i(0)\, e^{-\left(\frac{r}{a_t}\right)^2}$$

$$a_t^2 = \frac{3}{2}\, a_\ell^2\, \frac{q_o}{q_\ell} \qquad (5)$$

where a_ℓ is the limiter radius, q_o is central plasma safety factor and q_ℓ is the limiter q [12]. A computer program was written to numerically calculate the neutron spectrum for the Alcator C temperature and density profiles. Table 2 summarizes the correction factor as a function of q_ℓ. Note that over a wide range of q_ℓ the correction is quite constant. q_ℓ is proportional to I_p/B_t indicating the correction factor is very slightly dependent of the major plasma parameters. The reason for this can be understood by examining Fig. 4 and noting that for the region where the neutron production is important, $r < 6$ cm, the density is essentially constant. At 6.0 cm the density is 0.93 the central density. However, as can be seen in Table 2 the maximum neutron rate as a function of the minor radius does not occur at the center where the ion temperature is a maximum, but at about a minor radius of 2.3 to 4.0 cm (depending on q_ℓ) where the ion temperature is essentially constant at about 0.92 the central T_i. If the ion temperature profile broadens, the region

where the maximum production shifts with it while the temperature of the maximum production region remains constant. Thus the ion temperature derived from the half width of the neutron spectrum is insensitive to plasma profile effects.

Equation 5 does not however, include the effect of the 'sawtooth' oscillation which causes both spatial and time variations in the ion temperature. The sawtooth oscillation is caused by a plasma instability. In a short period of time the ion temperature profile flattens as in Fig. 5a. Figure 5b shows the neutron production profile and neutron spectrum just after a sawtooth crash. When the effect of the sawtooth oscillation is included the correction factor for the spatial effect is 0.84.

Combining the spatial and time effects, the measured T_i from the neutron spectrum width is 0.81 times the peak central T_i. This might vary as much as 10%, for arbitrary time limits, but varied less than 5% for the measurements presented below.

Table 3 summarizes values of the mean and dispersion for some plasma temperatures. Clearly, the shift of the mean energy is small compared to the change in the line width, and measurement of the line width is better suited to a temperature determination.

Using the results of table 3 for Alcator C ohmically heated plasmas for which the ion temperatures are typically 1.0 keV, a detector resolution better than 2.5% is required. This requirement greatly limits the choice of the detector. General discussions of neutron spectrometers can be found in references [13] and [14]. The ion chamber used here was found to have a resolution better than 2%. While many other techniques

have been proposed to measure the widths for higher temperature plasmas, [2], [15], [16], [17], [18], [19], no other technique has been found which has a sufficient resolution without a sacrifice of efficiency of several orders of magnitude. As will be seen below, the low efficiency of spectrometer, the short duration of the plasma discharge, (typically 400 msec), and the low neutron production rate make it necessary to sum spectra from many plasma discharges to obtain a useful spectrum.

II. The Spectrometer System

The spectrometer system shown in Figs. 6 and 7 consists of the high pressure ^3He ionization chamber [20] mounted in a shielding enclosure designed for the Alcator environment. The manufacturer of the ion chamber has provided a thermal neutron shield which is mounted around the ion chamber. This assembly is surrounded by a minimum of 1.0 cm of lead inside a double walled stainless steel box. The space between the walls of the box is filled with lightly packed Li_2CO_3 powder and an access port has been provided on one end to view the plasma. The port is blocked by a 1 mm thick sheet of cadmium to reduce the incoming thermal neutron flux. The stainless steel box is surrounded by a minimum thickness of 30 cm of Water Extended Polyester (WEP) [21]. The WEP is a mixture of 40% water, and 60% resin, with small amounts of boron or Li_2CO_3 used to capture thermal neutrons. A collimator, also made of WEP is used to limit the view of the spectrometer only to neutrons which pass through the "keyhole" of an Alcator C diagnostic port. This port allows a view of 4.4 cm by 26.0 cm through the 20 cm thick Bitter magnet used to provide the toroidal magnetic field.

Figure 8 is a block diagram of the spectrometer electronics. The

ionization chamber has an integrally mounted FET charge sensitive preamplifier. The preamplifier output is routed via a coax cable to a shaping amplifier. An 8 μsec time constant is used for pulse shaping. The amplifier output signal is direct coupled to a multi channel analyzer (MCA). Spectra are collected into 2048 channels with a conversion gain of 4096. A precision pulser provides a test signal onto the grid of the ion chamber. The capacitively coupled signal at the anode of the ion chamber is monitored to indicate noise on the signal. The amplitude of the pulser signal is adjusted to place the pulser peak in a channel above channel 1900, well above the range of interest for neutron spectrum counts. The MCA is interfaced to a PDP-11/T55 computer to provide archival of individual shots. Two high voltage supplies are used to supply the grid and anode voltages. The grid voltage was set to 847 volts and the anode voltage was set to 3000 volts as recommended by the manufacturer.

2.1 The Ionization Chamber

The ionization chamber has been described elsewhere in detail [22-29]. The chamber is a gridded type operating at a pressure of 3 atm of ^{3}He, 6 atm of argon and 0.5 atm of CH_4. In the detection process the neutron reacts via the $^{3}He(n,p)T$ nuclear reaction. This reaction has a positive reaction energy, Q, of 764.0 keV. The cross-section for this reaction is shown as a solid line and the competing elastic scattering cross-section is shown as a dotted line in Fig. 9. The open circles in Fig. 9 represent the spectrometer relative efficiency as reported by Franz et al. [26]. Note that the scattering cross-section is roughly three times larger than the reaction cross-section at 2.45 MeV. Further

the reaction cross-section increases as the inverse square root of the neutron energy. Thus the spectrometer is very sensitive to thermal and epithermal neutrons and will have contribution due the elastic scattering cross-section at all neutron energies.

The calibration spectrum shown in Fig. 10 illustrates the effect of the cross-sections on the detector response function. The source neutrons were produced by bombarding a deuterium target with a 140 keV deuteron beam. This source spectrum has an estimated width of 50 keV at FWHM and a mean energy of 2.42 MeV. There is a large component of thermal neutrons due to the return of thermalized neutrons from the room walls and floor. The spectrum is characterized by a) a full energy peak which results from reactions which deposit their full energy in the ion chamber, b) a thermal peak at zero neutron energy due to the large reaction cross-section for thermal energies, c) a recoil continuum from 0.75 times the neutron energy due to elastic scattering of the full energy neutrons on the ^{3}He gas d) a recoil spectrum due to the Hydrogen in the CH_4 gas, and, e) a γ ray continuum which is due to neutron capture and hard x-rays interacting in the ion chamber. The total energy deposited in the ion chamber is the sum of the Q of the $^{3}He(n,p)T$ reaction, 764 keV, and the incident neutron energy. Thus the thermal peak is offset by 764 keV and the signal due to gamma rays appears below the thermal peak. 2.4 MeV neutrons which react via the reaction cross-section but do not deposit their full energy in the active volume produce the continuum between the full energy peak and the first recoil feature.

Figure 11 shows a crossectional view of the known parts of the ion

chamber. The operation of a gridded ion chamber is described in Knoll [30]. In the commercial design the preamp is mounted at one end of the ion chamber to minimize pickup between the ion chamber and the FET of the preamplifier. The other end of the chamber provides a means of filling the chamber through a gas fill valve. A calcium purifier and heater has been provided to eliminate tritium from the ion chamber after extended use.

The manufacturer has included a thermal neutron shield consisting of 1 mm of cadmium and 3 mm of boron nitride powder around the active ion chamber volume. This shield is claimed to have a shielding effectiveness of 200 by the manufacturer.

2.2 Shielding and Collimation

In order to assess the amount and type of shielding required to shield the scattered neutrons the Monte Carlo Neutral Particle (MCNP) code [31] was used to study the neutron transport for the Alcator C machine geometry. The machine was modeled as a torus with the surrounding Bitter magnet plates. A single diagnostic port was modeled and tallies were made as a function of energy for positions at and away from the port. Figure 12 shows the neutron spectrum calculated for a position at a diagnostic port 50 cm from the plasma. Note that there is very little distortion of the 2.45 MeV source group. The small increase in the 2.3 to 2.35 MeV group would correspond to 180 degree scattering from copper, a major constituent of the Bitter magnets. The bulk of the scattered neutrons are at energies less than 0.1 MeV.

Because the ion chamber is very sensitive to thermal and epithermal

neutrons these results indicate that it is necessary to increase the amount of shielding over the manufacturers thermal neutrons shield. Further, in measurements done during plasma discharges with only the manufacturers shield the detector was saturated by the thermal and epithermal neutron flux. The code predictions indicated that the greatest number of neutrons are in the epithermal range, where the capture cross-sections are still ineffective. Thus, the decision was made to design the shield system to moderate and then capture the thermal neutrons.

A second consideration was to minimize the collimator opening so that the spectrometer viewed as little of the machine scattered neutron flux as possible. The horizontal access to the plasma is limited by the width of "key-hole" of the diagnostic port to approximately 4.4 cm. The vertical access is limited to 26.0 cm. It was shown earlier that the active length of the ion chamber is 14.9 cm and that the ion chamber's efficiency at detecting 2.45 MeV neutrons is insensitive to the ion chamber orientation as long as end on configurations are avoided. By placing the ion chamber at an angle of 20 degrees as shown in Fig. 7, a minimum collimator opening without loss of efficiency was obtained. The collimator opening was designed to be 5.08 cm horizontally and 10.2 cm vertically. This vertical opening was large enough so that the ion chamber viewed a large portion of the radial extent of the neutron producing part of the plasma. About ninety percent of the neutrons are produced inside a minor radius of 6.0 cm. The horizontal limit allows 5.3 cm of the total 402 cm circumference plasma to be viewed, or 1.2 percent of the total neutron producing plasma. The collimator opening is blocked by a 1 mm thick sheet of cadmium to remove thermal neutrons from the incoming neutron beam. The shield box was

designed so that there were no streaming paths.

Since the chamber is sensitive to gamma rays Li_2CO_3 powder was used as a thermal neutron capture material near the ion chamber. While natural lithium in this form is not as effective as boron compounds the capture of a thermal neutron by boron leads to a capture gamma of 0.48 MeV while the lithium capture reaction does not have a gamma ray associated with it. The Li_2CO_3 powder was lightly packed between the two stainless steel boxes. The packing density of the powder is 0.76 g/cc which is calculated to reduce thermal neutrons by at least two orders of magnitude. This thickness would correspond to a half value layer at 0.5 MeV. If greater thermal shielding is required, Li_2CO_3 enriched in ^6Li could be used.

Water Extended Polyester was chosen as the moderator because: 1. Shielding of any desired shape and size could be cast in house allowing a modular shield system to be used, 2. up to 40% of the weight could be water which is trapped in resin cells, and 3. Boric acid is soluble up to a 1.0 atom percent. Li_2CO_3 powder could be added also but had to be suspended in the resin making casting much more difficult. The shielding effectiveness of a 0.3 m thick block was tested by measuring the neutron spectrum for PuBe and Cf^{252} sources with and without a shield block in place. The shielding effectiveness was found to be approximately 30 for neutron energies above 1 MeV and to increase to about 100 at thermal neutron energies. The WEP shield has a total weight of 1070 kg.

The ion chamber is microphonic. To isolate the ion chamber approximately 50 kg of lead shielding was tightly coupled to the ion chamber, while the assembly was shock mounted on rubber cushions. One inch thick

pieces of soft foam rubber were used on each side of the 1 mm thick piece of Cd blocking the collimator port to further reduce acoustic pickup. When the WEP shield was in place around the shielding box no evidence of acoustic pickup was seen during acoustic noise tests simulating shot acoustics. Acoustic sensitivity was studied in detail by Franz et al. [26].

III. Spectrometer Performance

3.1 Energy Calibration with the $D(D,n)^3He$ Reaction

The energy calibration of the ion chamber was made with a D-D neutron generator. The accelerator is capable of accelerating deuterons to 140 keV with a beam current of 0.3 mA. Under these conditions up to 5.0×10^7 neutrons are produced per second. The spectrum was measured at a beam to neutron emission angle of 99 degrees where the dependence of the neutron energy on the ion beam energy is at a minimum. At this angle of 99 degrees the energy of the neutrons is 2.42 MeV. The error in this energy is estimated to be 10 keV and due to error in the measurement of the angle.

In order to determine the effect of the amplifier time constant, τ, on the detector resolution a series of spectra were measured at a beam angle of 99 degrees. Figures 13 and 14 show the results of this scan. In Fig. 13, one can see the qualitative effects. As the time constant is decreased the response function in the vicinity of the peak becomes more asymmetric and the FWHM increases. Figure 14 shows this effect as a plot of the increase in the FWHM as a function of the time constant. The data has been normalized to the 8 μsec value after which the

relative width appears to be constant. To maximize the possible count rate, the shortest possible time constant should be used. Here 8 μsec has been used since in most data taken to date the 8 μsec time constant has not resulted in excessive pile-up. Shorter time constants can be used if the loss of resolution is not important and if the asymmetry of the response function is corrected for.

3.2 Energy Resolution Calibration using the $^{7}Li(p,n)^{7}Be$ Reaction

Calibration neutrons were provided via the $^{7}Li(p,n)^{7}Be$ reaction which has Q value of -1644 keV. A proton beam from the Lawrence Livermore Laboratory's Tandem Van de Graaff Accelerator was used. The spectrometer was placed at a beam angle of 0 degrees. The protons had a mean energy of 4130 $\pm$ 25 keV and a dispersion of 3 keV. These conditions imply a neutron energy of 2450 $\pm$ 25 keV for the full energy peak.

The resolution of the spectrometer mounted in the primary shielding box was measured for neutrons incident on the spectrometer at angles of 20 degrees (parallel case) and 70 degrees (perpendicular case) to the ion chamber anode wire. The charge of the protons striking the target was collected to allow measurement of the relative efficiency of the parallel and perpendicular cases and an estimate of the intrinsic efficiency of the spectrometer. The active center of the spectrometer was placed at a distance of 70.2 cm for the parallel case and 113 cm in the perpendicular case. A LiF target of thickness 112 $\mu g/cm^2$ (8 keV) on a 40 mil tantalum backing was used.

Figure 15 shows the calibration spectrum for the parallel case. The data has been fitted with the function:

$$F(ch) = P_1 \, e^{-\frac{1}{2}\left(\frac{P_2 - ch}{P_3}\right)^2} + P_1 P_4 W \, e^{-0.707\left(\frac{P_2 - ch}{P_5}\right)} + P_6 W$$

$$W = \frac{1}{2} \, \mathrm{Erfc} \left[1 - \left(\frac{P_2 - ch}{P_3}\right)\right] \qquad (6)$$

Erfc is the Complementary Error Function and the p's are fit parameters. Note that the background and exponential are cut off by a complementary error function at the centroid of the Gaussian. For the spectrum shown the full width at half maximum (FWHM) of the component Gaussian is 38.2 $\pm$ 3 keV. The width of the fitted function is 45.6 $\pm$ 3 keV. The intrinsic efficiency for the parallel case was calculated to be $1.7 \pm 0.5 \times 10^{-4}$. The ratio of the intrinsic efficiency for the parallel case to the perpendicular case was measured by normalizing the ion chamber count rate to correct for the different source to detector distances and total run time. The ratio was found to be 0.98 ± 0.05. Thus the orientation of the ion chamber does not seem to be critical implying that the detector rate is dependent only on the number of neutrons passing through the active volume. However, because of the structure at either end, the ion chamber end configurations will result in a loss of efficiency.

3.3 Figures of Merit

Because good resolution requires a long time constant and tokamak plasma shots are typically less than one second in duration, it is important to quantify the maximum allowable count rate. A useful figure of merit is the ratio of the number of counts in the full energy peak to the total number of counts in the neutron spectrum. Formally, the integral of the number of counts between the full width at tenth maximum is compared with the integral of counts in the total spectrum. It should be noted that for all these comparisons an arbitrary cut off is used on the low energy side. This lower limit corresponds to the cutoff from the lower level discriminator on the multi channel analyzer. This cut off would correspond to an energy of less than 500 keV deposited in the ion chamber. The energy could be from gamma or neutron interactions. The typical value for this figure of merit is 1/70. Thus, one out of every 70 detected pulses recorded in the MCA is a full energy peak pulse.

A second figure of merit is the total count rate. Here a distinction must made between the ionization chamber count rate and the MCA count rate. The MCA count rate does not include the pulses cut off by the lower level discriminator. Because the number of gamma rays varies significantly with the type of plasma discharge, there can be significant differences between the two rates. The effect the type of discharge and gamma ray level will be discussed further below. The manufacturer and various authors [2,22,24,26] have indicated that the maximum count rate is 10^4 counts per second. However, it is the electronic pulse system which limits the count rate. If the time constant of the pulse shaping is reduced the count rate limitation will increase.

(At a cost of resolution, as was shown in Fig. 13.) This maximum count rate is also sensitive to where the MCA lower level discriminator is set. The MCA count rate will not include pulses which fall below the lower level discriminator and the number of pulses increases sharply in the lower energy channels. Thus the count rate at the MCA can vary significantly with the lower level discriminator setting. Further the number of gamma rays and hard x-rays varies significantly with the type of plasma discharge, and the pulse amplitudes for photon interactions are generally below the discriminator level, so there can be significant variation due to the gamma ray background. Thus, the MCA count rate is always less than the rate at which radiation interacts in the ion chamber. The authors above have all used different lower discriminator settings and amplifier time constants. More important is the amount of pile-up on the peaks in the spectrum. This effect is insensitive of the MCA discriminator level. For the discriminator level we have chosen, the pile-up effects are minimized and the MCA dead time is below 2%. This would correspond to a total count rate of about 4×10^3 per second for the 8 μsec time constant used.

IV. Measurements at Alcator C

A typical plasma discharge or shot for Alcator C is shown in Fig. 3. For the shot shown the field was 8 T and the plasma current was 375 kA. The maximum electron density was $3 \times 10^{20} m^{-3}$.

The neutron rate signal is derived from a bank of 14 one inch diameter ^3He proportional counter tubes whose current is summed through an operational amplifier. The shaded region indicates the time during which the spectrometer is gated on.

Such a plasma discharge produces 10^{10} neutrons. Unfortunately only about one out of every 7×10^9 of the total number of neutrons produced in the plasma contributes to the full energy peak due to solid angle losses and the low detection efficiency of the ion chamber.

Neutron spectra were collected for individual plasma discharges and stored on magnetic media for later analysis. Typical 2.45 Mev peak counts rates were only a few per shot requiring a large number of similar shots to be summed together to obtain useful spectra. The best single shot analyzed to date had a peak rate of 2×10^{11} neutrons per second. During the 250 msec on time there were 11 neutrons collected in the full energy peak or a peak count rate of 44 per second. This is very close to the maximum rate at which the spectrometer can operate for the 8μsec amplifier time constant used. The dead time was estimated to be 2% on that shot and the thermal peak was not distorted. By reducing the amplifier time constant and using a pile-up rejecter a count rate as high as a 100 per second appears to be an upper limit on the count rate.

In practice, it is necessary to sum a large number of similar plasma discharge spectra together to deduce useful information on the plasma. In Fig. 16, 303 plasma discharges have been summed together in order to understand overall properties of the spectrometer performance. Two calibration spectra and a sum of a single day, 62 plasma shots are also shown. It is clear from Fig. 16 that there is a peak at 2.45 MeV. Further there is little or no contribution to the spectrum from neutrons produced by photonuclear reactions, electrodisintegration, photodisintegration or neutron down-scattering from the machine structure. Quantitatively, the number of counts in an integral containing the peak to an

integral of counts in the lower channels has been compared for both the calibration spectrum and the shot data. Table 4 shows the results of this comparison. In the first case, a $D(D,n)^3He$ calibration, the shield including the WEP was assembled in the accelerator room. In the second case in table 2 the integrals for a spectrum were taken using the D-D reaction but without the WEP moderator. The fifty fold increase in the ratio is due to the high level of room return. The accelerator vault has one meter thick concrete walls. The nearest wall was only 200 cm away and the floor was only 60 cm away. The source to detector distance was 96 cm. The comparison of these tests indicate how important the WEP is to the shield effectiveness. A further test of the shield effectiveness was performed by blocking the collimator with a 10 cm polyethylene block during typical plasma discharges. A total of 11 neutron counts in the entire spectrum were recorded compared to an average of 86 counts recorded for the unblocked case. Assuming a mean free path of 2.5 cm for fast neutrons in the polyethylene block a 6% transmission is expected. This is consistent with the test results. For the Li(p,n)Be calibration case the WEP moderator was not used, but the facility has a false floor allowing the spectrometer to be at least 500 cm from the nearest wall or floor while the source to detector distance was 70 cm. Thus the spectrum would be expected to be dominated by the direct flux. The small peak near 2.0 MeV is due to an excited state of Be. The integrals for a series of spectra sums are similar to the calibration results and indicate that the fusion spectra are dominated by 2.5 MeV neutrons.

V. Determination of the Ion Temperature

To deduce the ion temperature from the line width of the peak the following procedure was used:

1. The thermal and pulser peaks were examined on an individual shot basis to reject bad shots.
2. Plasma spectra measured under similar conditions were summed to obtain sufficient statistics.
3. The pulser and thermal peaks were fitted using a Gaussian function to determine the noise during the set of summed shots.
4. The full energy peak was fitted and the error of the fit was determined as described below.
5. The fitted width was corrected for the detector resolution and for noise broadening of the peak.
6. The average ion temperature was determined using equation 3 and corrected as described earlier to obtain the central peak ion temperature.

The primary criteria for rejecting a plasma shot was a loss of more than 4 counts from a normal 20 counts in the pulser peak during the 200 msec spectrum measurement of a plasma shot. The most probable cause of the loss of pulser counts was the pile-up due to hard x-rays and photoneutrons produced at the limiter where the most difficulty with pileup was encountered. A ring of molybdenum blocks is used to limit the extent of the plasma minor radius at two toroidal locations at Alcator C. The level of photoneutrons and gamma rays is a strong function of how the gas is added to the plasma discharge at the start of the discharge. Further, in preliminary tests at a non-limiter port, very few shots had to be rejected due to pile-up of gamma and photoneutron counts. The measurements reported below were done at a port with a limiter and great care was taken in the gas programming to avoid high photo-neutron and hard x-ray levels.

The summing of the data was accomplished by simply adding spectra on a channel to channel basis. This procedure was allowed only because the absolute channel drift was less than one channel per day and less than 3 channels per week.

The pulser and thermal peaks were fitted in a least squares fashion with a single Gaussian function. The contribution to the peak width from ion chamber noise pick-up during the shot was typically 40 keV for a sum of shots.

As mentioned above, spectra were recorded into 2048 channels, or approximately 70 channels across the full energy peak. While the normal procedure is to collapse the data until only four to five contain the half width of the peak and then fit a function minimizing the Chi Square statistic, Cash [32,33] has suggested that more information is gained if the original un-collapsed data is fitted using the 'C' statistic. It is necessary to abandon the Chi-square statistic because of the requirement that the standard deviation of the number of counts in any channel be equal to the square root of the number of counts. This is not true when the number of counts is less than 10 as is the case here. The 'C' statistic is simply

$$C = 2 \sum_{i=1}^{N} [e_i - n_i \ln(e_i)] \qquad (7)$$

where n is the number of counts in a channel, N is the number of channels and e is the expected number of counts from the fitted function. Confi- Confidence intervals are generated by varying the parameter of interest around the best fitted value. The value of C for the minimum case is then subtracted from the C found for varied value. Cash has shown that

this difference is distributed statistically as a Chi square distribution with one degree of freedom. Thus a confidence can be generated from the ΔC. Figure 17 shows the confidence of fit as a function of Gaussian component sigma using the technique of Cash for data taken on the 6th of August, 1982. Such a curve can be used to determine the range of σ about a best estimate of σ given a required confidence. A 68% confidence interval has been used for error analysis here. Using this technique shots with as few as 20 counts in the peak have been analyzed. However, it was necessary to have at least 150 counts in the peak to obtain 20% error bars on the ion temperature deduced from the width.

In order to assess whether the width could be used to deduce the ion temperature, two sets of plasma shots were analyzed. The plasma conditions are summarized in Table 6. Note that in the low plasma ion temperature (low T_i) case the peak ion temperature is estimated to be about 800 eV and 1050 eV in the high T_i case. These temperature estimates are based on the total neutron rate and neutral particle charge exchange diagnostics. Both these diagnostics are reported to have measurement uncertainties on the order of 10%. The shot to shot variation of these derived temperatures was on the order of 10 to 15%.

Figure 18 shows the two data sets after groups of 9 channels of data have been added together for presentation purposes. The functional form of the fitting function is equation (6) above with parameters p4 and p5 fixed from the calibration. The optimal fit from the 'C' statistic normalized to the peak height is shown for the low T_i case. Even in this data which has not been corrected for the noise or spectrometer resolution, the high T_i case has a greater width. The calculated ion temperature is shown plotted against the total neutron rate and charge

exchange derived ion temperatures in Fig. 19. The dotted line would represent perfect agreement. Note that measurements are consistent with the theoretically expected result.

VI. Summary

The neutron spectrometer system described here has been used to measure the neutron spectrum at Alcator C. The spectrometer resolution has been measured to be 46 keV FWHM and the absolute energy calibration is accurate to 10 keV. By utilizing the structure of the Alcator C magnet in the collimator and shielding design an effective rejection of unwanted neutron and gamma ray counts has been accomplished. Furthermore, the shielding and collimator system is modular allowing it to be assembled at any Alcator C horizontal diagnostic port with normal laboratory lifting equipment. All materials used are readily available and the primary shielding material, WEP, can be cast and machined with relative ease. The ion chamber used is also commercially available.

While the spectrometer has very good energy resolution it appears to be count rate limited to less than 100 counts in the 2.45 MeV peak per second. This is an improvement over the measurements of Strachan et al. [2]. For the measurements done here, the count rate was limited by the production rate from the Alcator C plasma and many plasma shots had to be summed to obtain a usable spectrum. Even if the neutron production rate in the plasma is increased it will be necessary to accumulate at least several seconds of 'on' time. Thus, at least 10 typical Alcator C discharges would be required. If discharge durations are extended or if several ion chambers are used in parallel this requirement could be relaxed.

The measurements done to date at Alcator C indicate that the spectrometer is quite easy to use in the tokamak environment. No special magnetic shielding was incorporated in the design, and signals were routed over standard 50 Ω coaxial cable from the preamplifier to the shaping amplifier. Nevertheless, noise pickup during the plasma shot contributed only an equivalent of 40 keV to the pulser and thermal peak widths and could be corrected for. Table 5 provides a summary of the spectrometer performance.

By summing shots together it has been possible to determine ion temperatures from the widths of the thermonuclear peaks. This is the first case known to us in which the ion temperature has been determined from the peak width for an ohmically heated discharge and also the first systematic test of the technique against other ion temperature diagnostics. The spectrometer is expected to be extremely useful for the study of plasmas with non-thermal ion energy distributions.

We would like to thank the support staff of the MIT Alcator C fusion group, Francis Bitter Magnet laboratory, and MIT Reactor machine shop for their assistance. We would also like to thank Dr. D. Slaughter at the Lawrence Livermore Laboratory for his help in the calibration of the ion chamber, and Frank Chmara of Peabody Scientific for his help in conjunction with the ion chamber.

This work was supported by U.S. Department of Energy Contract No. DE-AC02-78ET51013.

REFERENCES

1. G. Lehner and F. Pohl, "Reaktionsneutronen als Hilfsmittel der Plasmadiagnostik", Zeitschrift für Physik 207 (1967) 83-104.

2. J. D. Strachan, et al., Nature (London) 279 (1979) 626-628.

3. J. D. Strachan and D. L. Jassby, Trans. Am. Nucl. Soc. 26 (1977) 509.

4. W. A. Fisher, "D-D Fusion Neutron Spectra Measurements and Ion Temperature Determination at Alcator C". M.I.T. Plasma Fusion Center Report PFC/RR-83-3.

5. "Studies of the Photonuclear Neutron Emission During the Start-up Phase of the Alcator C Tokamak", D. S. Pappas, R. Furnstahl, G. P. Kochanski, PFC/RR-81-22, May 1981.

6. H. Knoepfel and D. A. Spong, Nucl. Fusion 19 (1979) 785-829.

7. R.E. Chrien "Measurement of Fusion Reactions from a Tokamak Plasma", Ph.D. Thesis, Dept. of Astrophysical Sciences, Princeton University, 1981.

8. G. Lehner in Reactions under Plasma Conditions, Vol II, edited by M. Venugapalan, John Wiley and Sons, 1971, 509.

9. T. Elevant, Nucl. Instrum. Methods 185 (1981) 313-320.

10. H. Brysk, Plasma Phys. 15 (1973) 611.

11. M. M. R. Williams, J. Nucl. Energy 25 (1971), 489-501.

12. Fairfax et al., "Energy and Particle Confinement in the Alcator Toka-

maks", IAEA-CN-3/N-6.

13. Calvert and Jaffee in Fast Neutron Physics, Part II edited by Marion and Fowler, John Wiley and Sons, 1980.

14. G. Knoll, Radiation Detection and Measurement chapt. 15, John Wiley and Sons, 1980.

15. D. R. Slaughter, IEEE Trans. Nucl. Sci. NS-26 (1979) 802-808.

16. H. W. Hendel et al., "Tokamak Fusion Test Reactor Fusion-Reaction-Products Diagnostics" presented at the Fourth ASTM-EURATOM Symposium on Reactor Dosimetry, NBS, March 1982. (Unpublished)

17. M. Chatelier et al., Nucl. Instrum. Methods 190 (1981) 107-118.

18. TFR Group, in 8th Conf. Controlled Fusion and Plasma Physics, 1 (1977) 1.

19. R. A. Lerche et al., Appl. Phys. Lett. 31 (1977) 645.

20. Model FNS-1, Seforad-Applied Radiation, LTD., Israel.

21. Manufactured by Ashland Chemical, Ohio.

22. Instrument Manual for Seforad Fast Neutron Spectrometer, Model FNS-1 Seforad-Applied Radiation LTD. Emekhayarden, Israel.

23. J. Cuttler, et al., Trans. Am. Nucl. Soc. 14 (1971).

24. A. E. Evans, J. D. Brandenberger, "High Resolution Fast Neutron Spectrometry without Time-Of-Flight", LA-UR 78-2562 (1978).

25. S. Shalev, J. M. Cuttler, Nucl. Sci. Eng. 51 (1973) 52-66.

26. H. Franz et al., Nucl. Instrum. Methods 144 (1977) 253-261.

27. W. C. Sailor, S. G. Prussin, Nucl. Instrum. Methods 173 (1980) 511-515.

28. S. G. Prussin et al., Nucl. Instrum. Methods 173 (1980) 505-509.

29. G. Rudstam, Nucl. Instrum. Methods 177 (1980) 529-536.

30. G. Knoll Radiation Detection and Measurement, p.178, John Wiley and Sons, 1980.

31. MCNP - A General Monte Carlo Code for Neutron and Photon Transport, Version 2B, LA-7396-M revised April, 1981.

32. W. Cash, Astron. Astrophys. 52 (1976) 307-308.

33. W. Cash, Astrophys. J. 228 (1979) 939-947.

Machine Parameters	Design	to date	unit
Major radius	64	58 to 71	cm
Minor radius	16.5	10 to 16.5	cm
Toroidal field	140	30 to 130	kG
Current	1000	100 to 750	kA
Density	$2x10^{21}$	$1x10^{19}$-$1.3x10^{21}$	m^{-3}
Aux heating			
4.6 Ghz Lower Hybrid	4000	0 to 750	kW
150-200 Ghz Ion Cyclotron	4-10	0	MW

Table 1. Alcator C Operating parameters.

q_{lim}	r_{max}	$T_i(r_{max})$	T_i from width
2.00	3.5	0.928	0.863
2.50	3.2	0.924	0.860
3.00	2.9	0.926	0.858
3.50	2.7	0.925	0.856
4.00	2.6	0.921	0.855
4.50	2.4	0.924	0.855
5.00	2.3	0.922	0.854
5.50	2.2	0.922	0.854
6.00	2.1	0.923	0.853

Table 2. Correction factor versus q_{lim}.

plasma temperature (keV)	mean energy (keV)	width FWHM (keV)
0.5	2453	58.2
1.0	2455	82.5
1.5	2456	100.8
2.0	2458	116.4

Table 3. Mean neutron energy and peak line width versus the plasma temperature.

Case, File	Notes	integral 1250-1400	integral 800-1250	ratio
19aprc.270	$D(D,n)^3He$ full shield	2896	4166	1.44
31janc.253	$D(D,n)^3He$ no WEP, high scatter	252	13107	52.0
18augc.282	Li(p,n)Be no moderator, low scatter	16139	29946	1.86
super6.um1	sum of 303 plasma discharges	846	1174	1.39
06augs.um5	sum of 62 plasma discharges 8-6-82	101	114	1.13

Table 4. Ratio of counts in peak integral to below peak integral.

1. The energy resolution is 46 keV at FWHM at 2450 keV.

2. The energy calibration is accurate to 10 keV at 2450 keV.

3. The contribution to the peak width due to noise pickup during a plasma shot can be measured, allowing the peak width to be corrected for the noise contribution. A typical value at FWHM is 40 keV .

4. The ratio of counts in the full energy peak to total ion chamber counts is 1/70.

5. The maximum count rate to date is 44 counts per second in the full energy peak. The ultimate achievable D-D neutron peak count rate is estimated to be less than 100 counts per second.

6. The intrinsic efficiency of the ion chamber is measured to be $1.7 \pm 0.5 \times 10^{-4}$ at 2.45 MeV.

7. The collimator and shielding design utilizes the Bitter magnet in its design. The system is modular in design, allowing the spectrometer to be used at any horizontal port. The shield weight is approximately 1 metric ton.

Table 5. Summary of Spectrometer Performance.

	"Low" T_i case	"High" T_i case	unit
number of shots	169	38	
plasma current	350-400	550-625	kA
toroidal field	80	110	kG
line averaged density	2.5×10^{20}	2.3×10^{20}	m^{-3}
T_i from neutron rate and charge exchange	780	1050	eV

Table 6. Plasma conditions for "low" and "high" T_i cases.

FIGURES

Fig. 1. The Alcator C fusion device. The plasma is confined in the vacuum chamber by the effect of the toroidal magnetic field and ohmic heating current. A typical plasma limiter consisting of a ring of molybdenum blocks is also shown.

Fig. 2. The neutron spectrum which would result for a plasma which exhibits all the observed significant neutron producing reactions in an Alcator deuterium plasma discharge.

Fig. 3. A typical high Alcator C plasma discharge as illustrated by three plasma diagnostics. Top, plasma current, middle, line average density from laser interferometer, bottom, neutron production rate. Toroidal field was 8.1 Tesla. The shaded region represents the time during which the neutron spectrum was measured.

Fig. 4. Neutron production at a given plasma radius and neutron spectrum expected after integrating over the entire plasma. Top, neutron production, solid line, ion temperature profile, dotted line. The ion temperature is assumed to be zero at the plasma limiter, r = 16.5 cm. Bottom, neutron spectrum. The width is obtained by subtracting 2450 keV from the calculated neutron energy.

Fig. 5a. Model of the plasma ion temperature distribution before and after a sawtooth crash. Solid line, before crash, dotted line after crash. r_s is the surface at which the plasma q = 1.

Fig. 5b. Neutron production rate versus radius and corresponding neutron spectrum for a plasma just after a sawtooth crash.

Fig. 6. Top view of neutron spectrometer next to the Alcator C device. Cross-section is through the mid-plane of the machine. In this geometry, approximately 1% of the total plasma volume is viewed.

Fig. 7. Side view of the neutron spectrometer.

Fig. 8. Spectrometer electronics. Standard NIM electronics have been used.

Fig. 9. ^{3}He elastic, (n,p) cross-sections and relative efficiency of ion chamber. Efficiency data taken from Franz et al. [24]. Cross-section curves from ion chamber users manual [20].

Fig. 10. Ion chamber response function. Source neutrons were produced from a 140 keV deuterium beam striking a deuterated titanium target. The spectrometer was at an angle of 99° to the beam direction where the neutron energy is 2.42 MeV with a dispersion of about 0.05 MeV. The pulser and thermal peak features have been reduced in magnitude for presentation.

Fig. 11. Crossectional view of ion chamber illustrating the ion chamber structure which inhibits the use of the ion chamber in an end-on configuration.

Fig. 12. Calculated neutron spectrum resulting from a monoenergetic 2.45 MeV distributed source using the MCNP (Monte Carlo Neutral Particle) code for the Alcator C geometry. The spectrum is for a position 50 cm from the plasma, at a diagnostic port.

Fig. 13. Qualitative effect of the pulse amplifier shaping time

constant. Spectra were taken with a neutron source energy of 2.42 MeV and an energy dispersion of about 50 keV using a 140 keV deuteron beam on a deuterated titanium target. The gain of the amplifier varies with the time constant.

Fig. 14. Quantitative effect of the amplifier time constant on the width of the peak FWHM normalized to the 8 μsec time constant case. The effect of the source width (~50 keV) has not been removed and is roughly equal to the detector resolution for the 8 μsec case.

Fig. 15. Calibration peak and fit due to the Li(p,n)Be reaction. A thin Li target was used so that the source dispersion is less than 25 keV. An 8 μsec amplifier time constant was used and the FWHM = 46 keV.

Fig. 16. Neutron spectra. Top left, spectrum from a D(D,n)T reaction. Bottom left, due to Li(p,n)Be reaction. Top, right, a sum of 303 plasma discharges. Bottom, right, 62 plasma discharges of a single day. The small peak in the Li(p,n)Be case is due to an excited state of Be. Note the similarity of the spectra indicating that the neutrons from an Alcator plasma are dominated by the D-D 2.45 MeV neutrons.

Fig. 17. Confidence of the fit for a given σ (width) of the Gaussian component of the fit. The method outlined by W. Cash has been used here. Standard (one sigma) uncertainty can be obtained by using the values of σ at the 68% percent confidence level.

Fig. 18. Nine channel collapse of peak data for low and high T_i cases. Note the greater width for the high T_i case (top) evident even in data which has not been corrected for the detector resolution or system noise. The curve on the low T_i data, (bottom) is the fit obtained using the C-statistic minimization, normalized for collapsed data magnitude.

Fig. 19. Reduced width of the 2.45 MeV fusion peak and corresponding temperature plotted against the central ion temperature determined from the total neutron rate and neutral particle charge exchange diagnostics. The dotted line shows the expected dependence. The scale on the right can be used to convert the width to a central ion temperature.

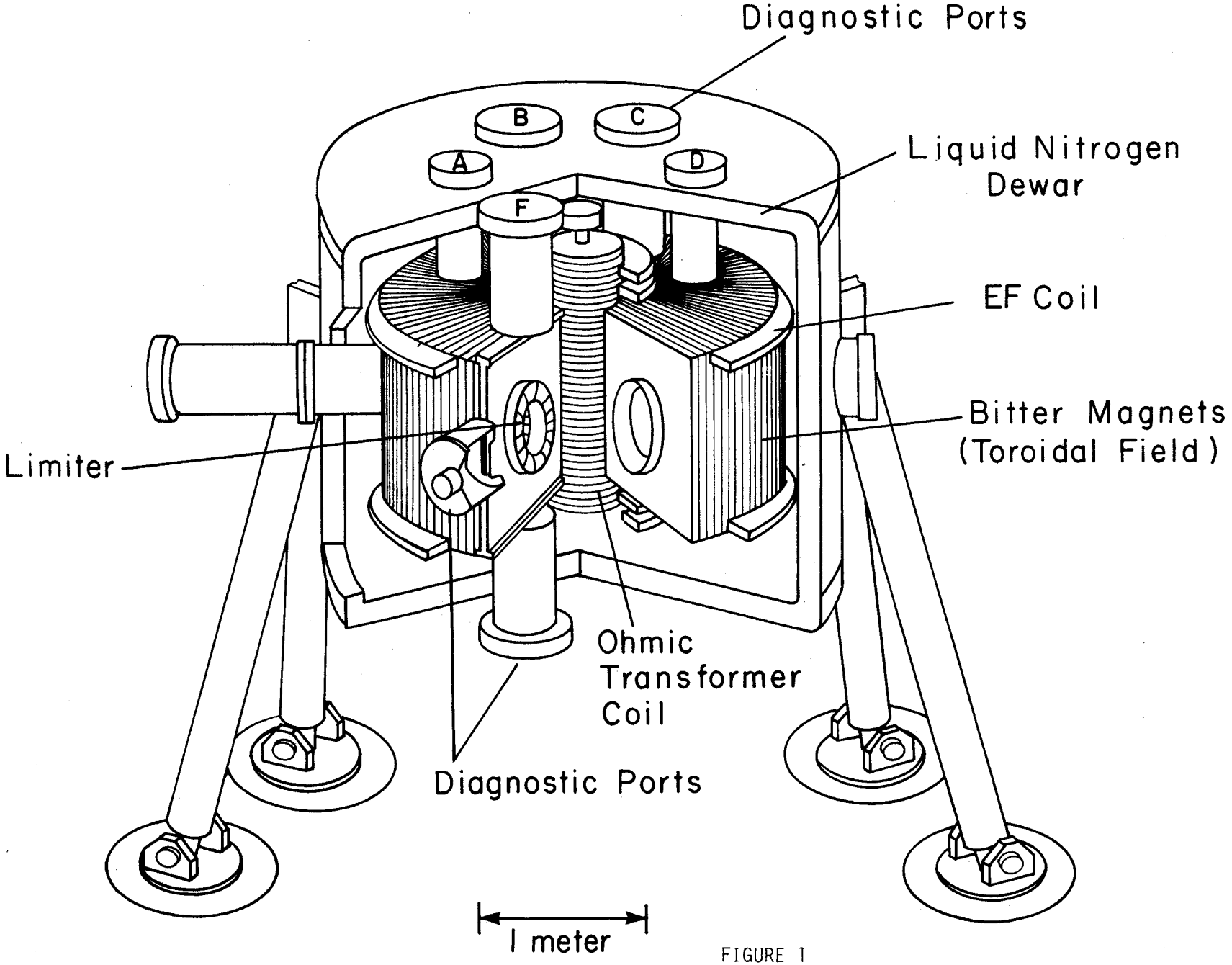

FIGURE 1

PFC-8295

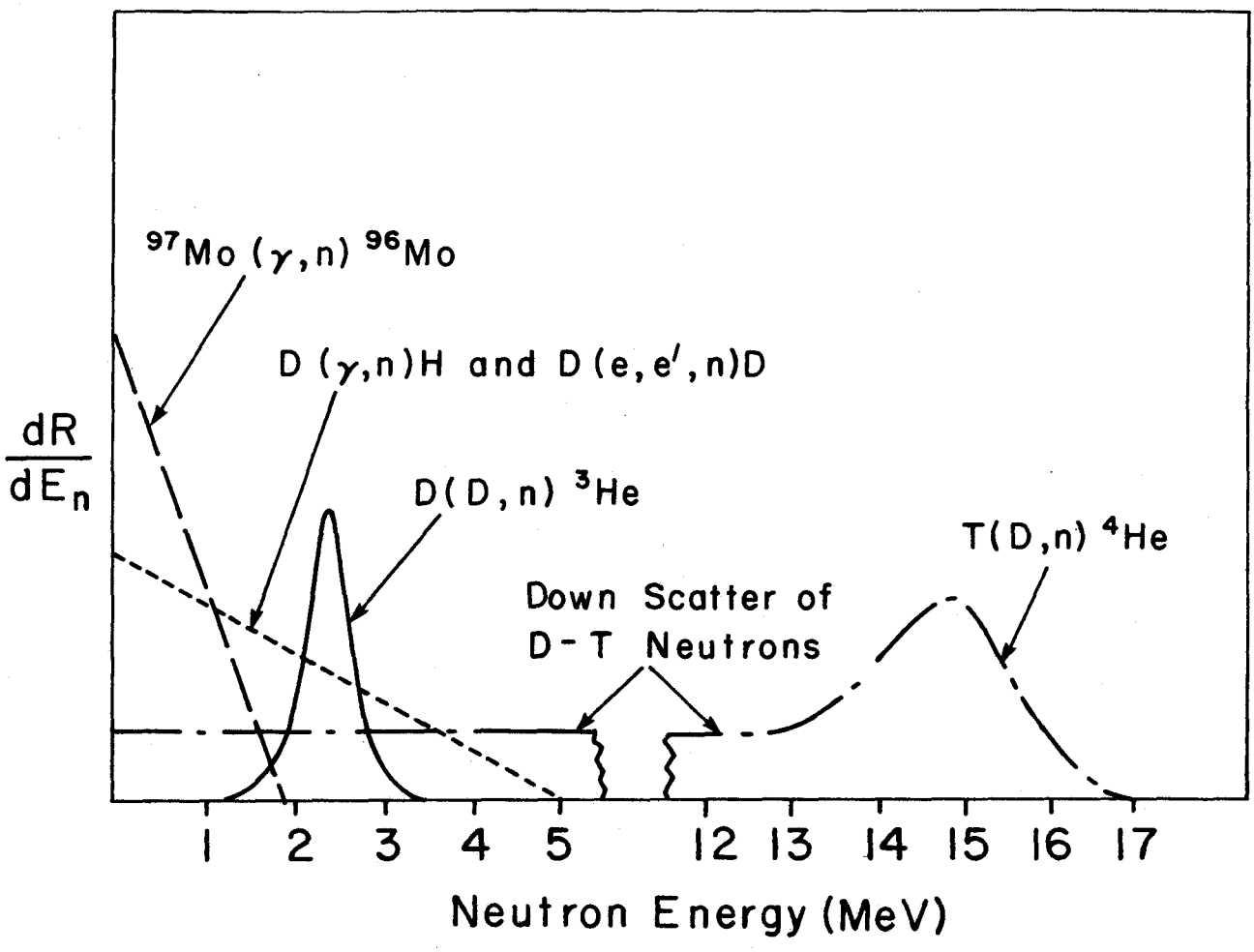

PFC-8353

FIGURE 2

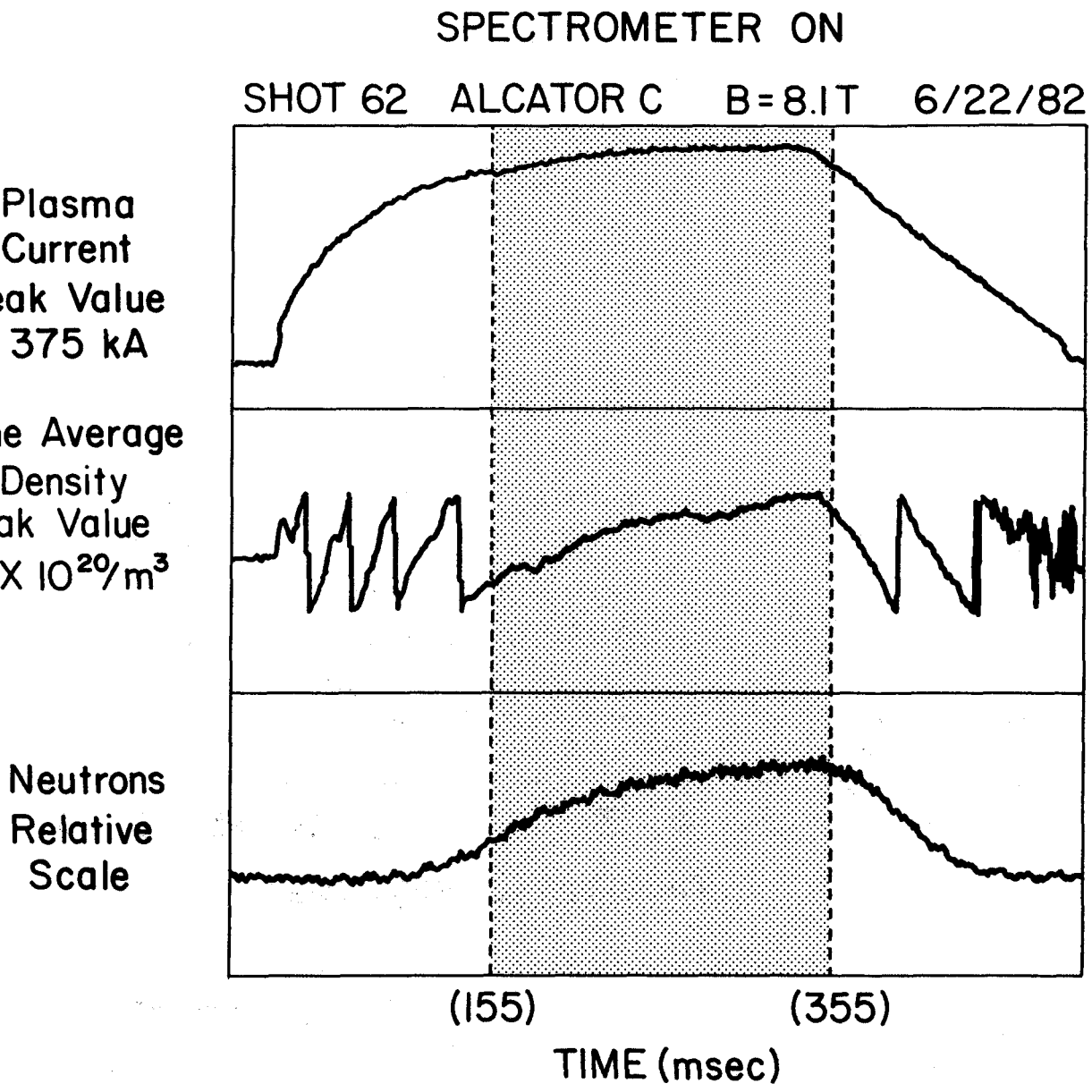
SPECTROMETER ON
SHOT 62 ALCATOR C B=8.1T 6/22/82
Plasma Current
ak Value
375 kA
e Average
Density
ak Value
X 10²⁰/m³
Neutrons
Relative
Scale
(155)
(355)
TIME (msec)
PFC-8118

FIGURE 3

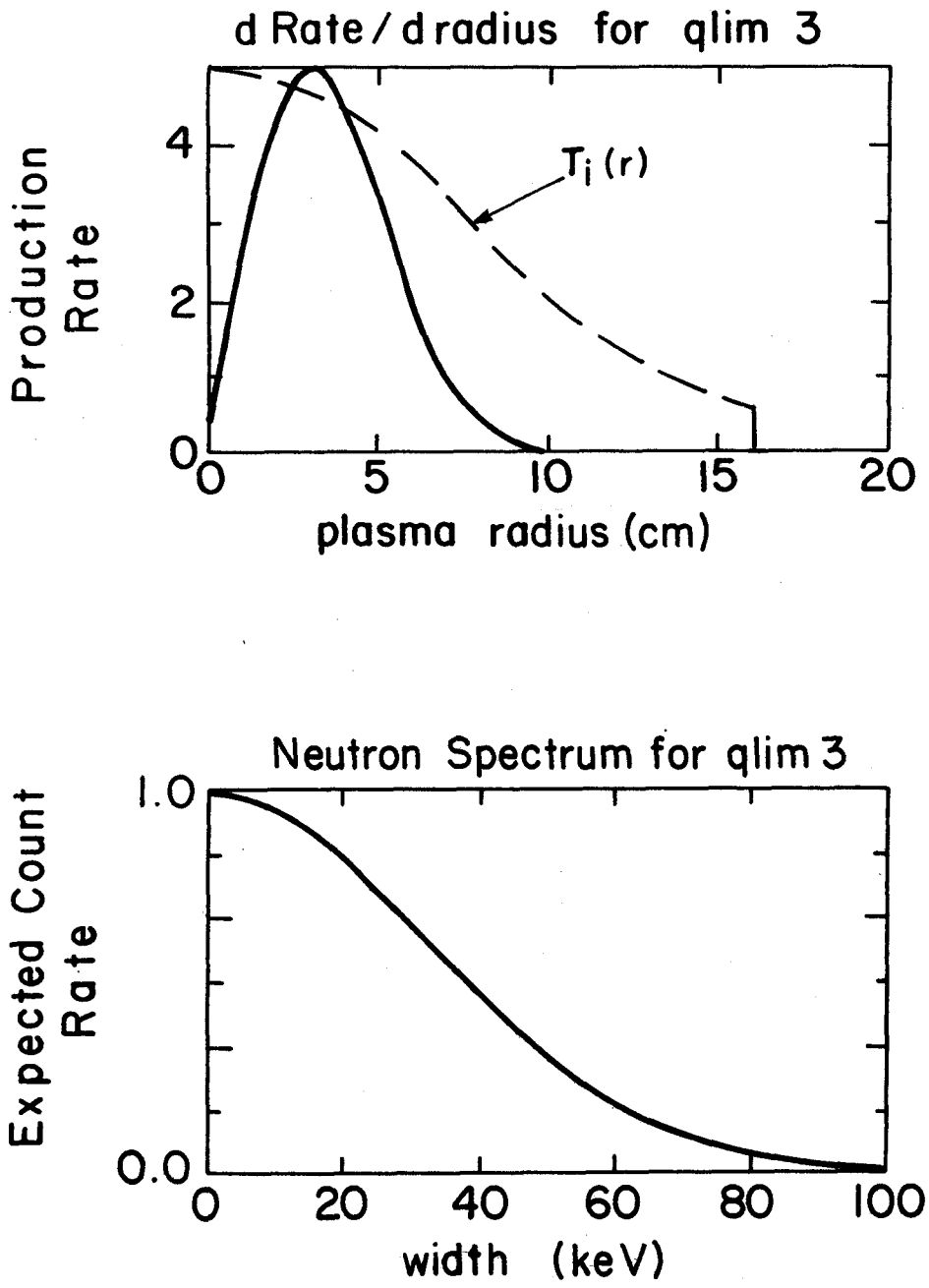
d Rate / d radius for qlim 3
Production Rate
4
2
0
T_i (r)
0
5
10
15
20
plasma radius (cm)
Neutron Spectrum for qlim 3
Expected Count Rate
1.0
0.0
0
20
40
60
80
100
width (keV)
PFC-8116

FIGURE 4

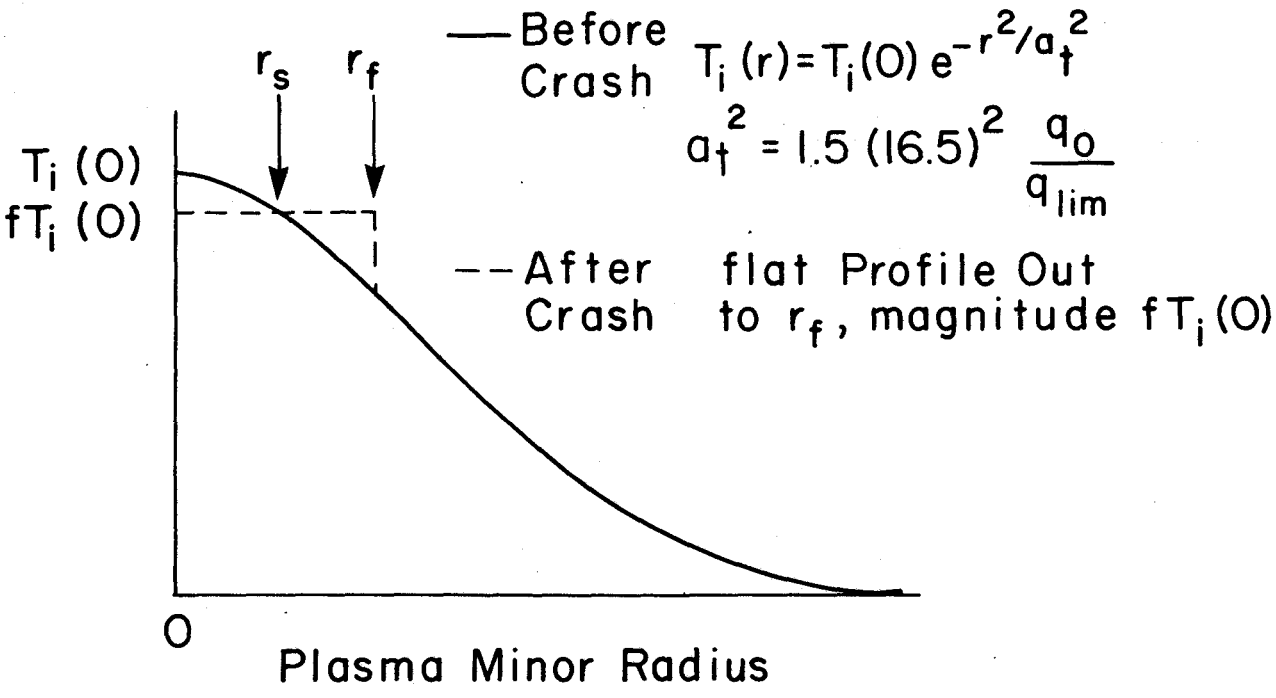

PFC - 8355

FIGURE 5a

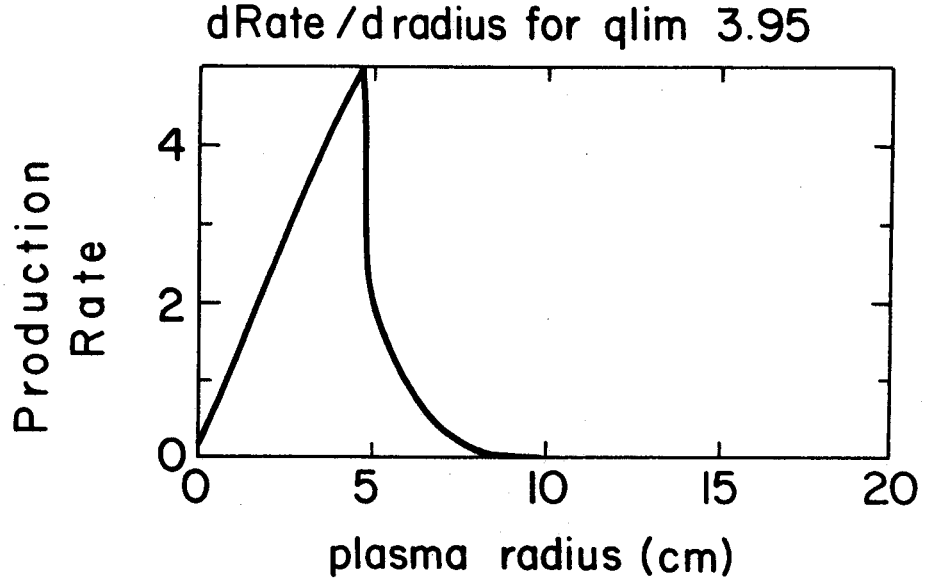

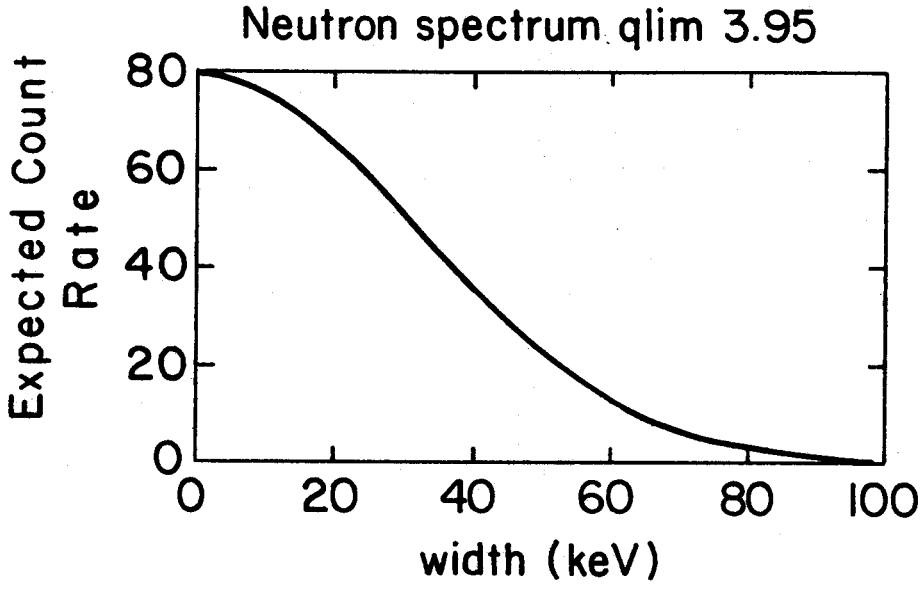

PFC-8352

FIGURE 5b

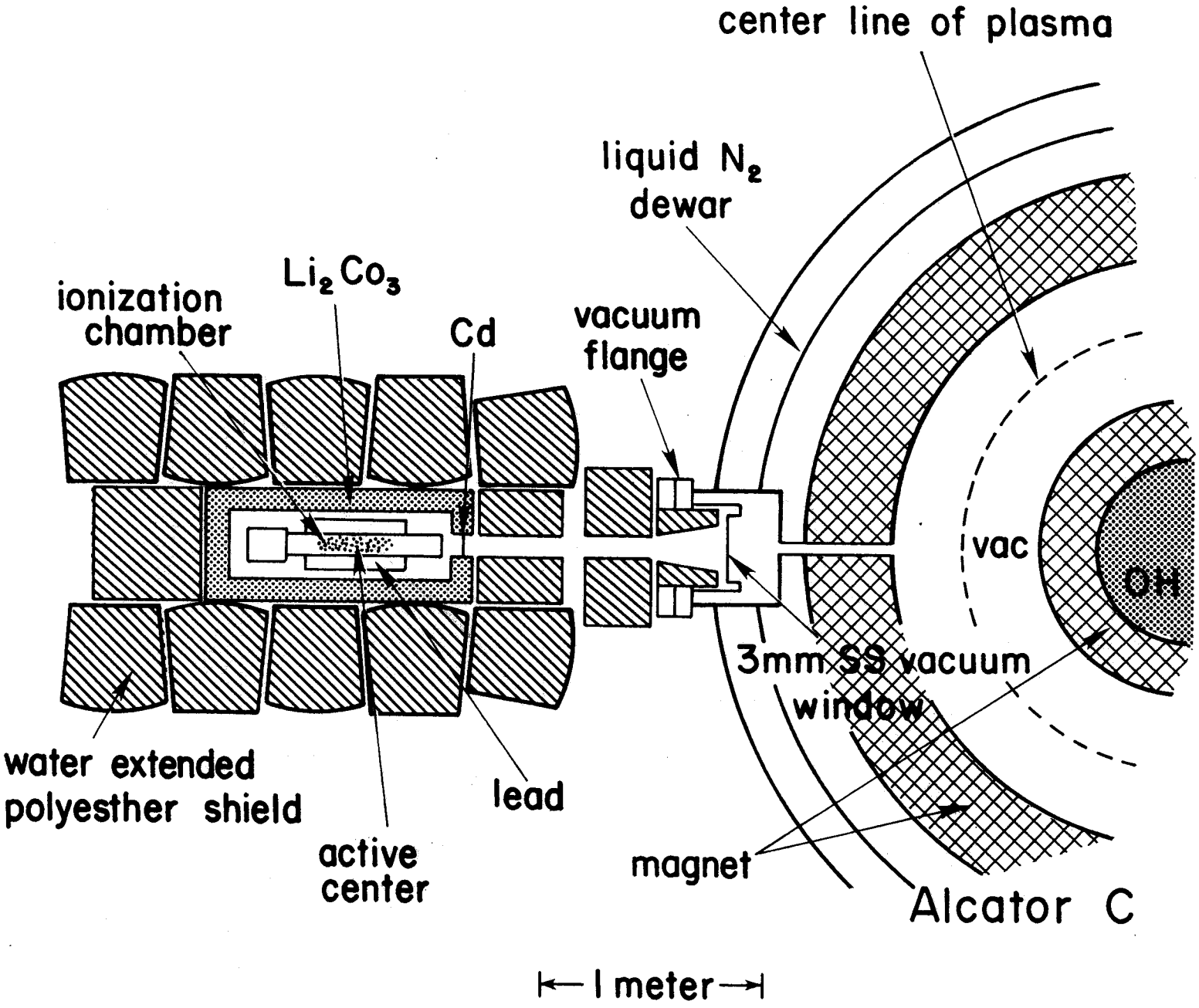

FIGURE 6

PFC-8110

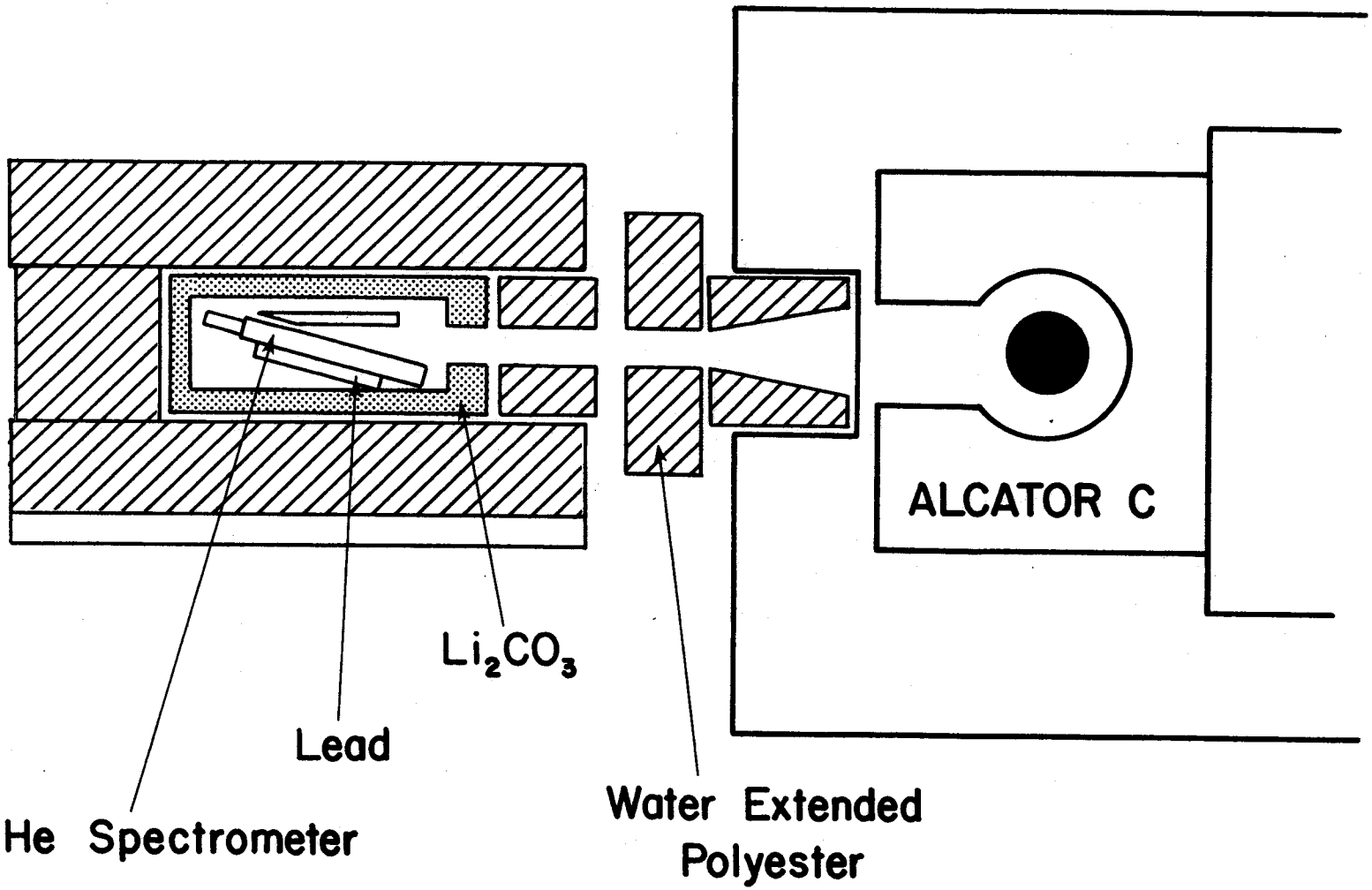

FIGURE 7

PFC-8123

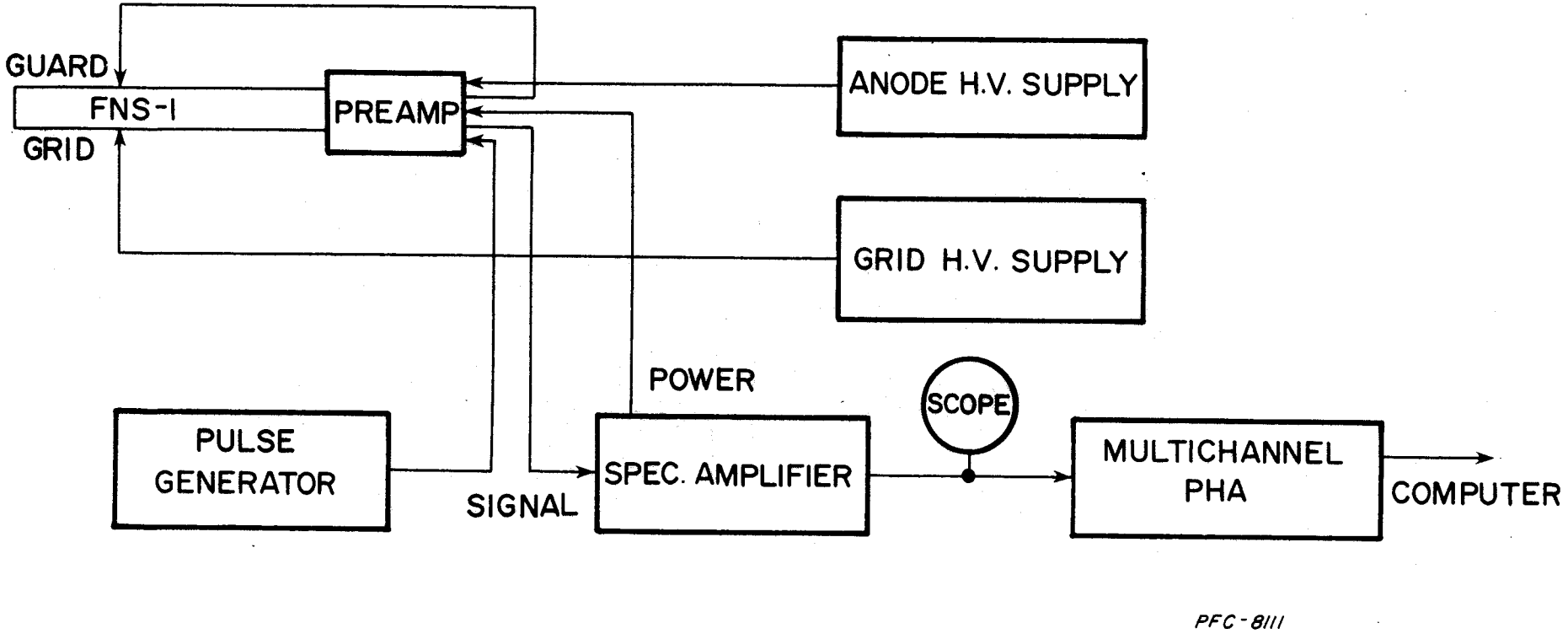
GUARD
FNS-I
GRID
PREAMP
ANODE H.V. SUPPLY
GRID H.V. SUPPLY
POWER
SCOPE
PULSE GENERATOR
SIGNAL
SPEC. AMPLIFIER
MULTICHANNEL PHA
COMPUTER
PFC-8111

FIGURE 8

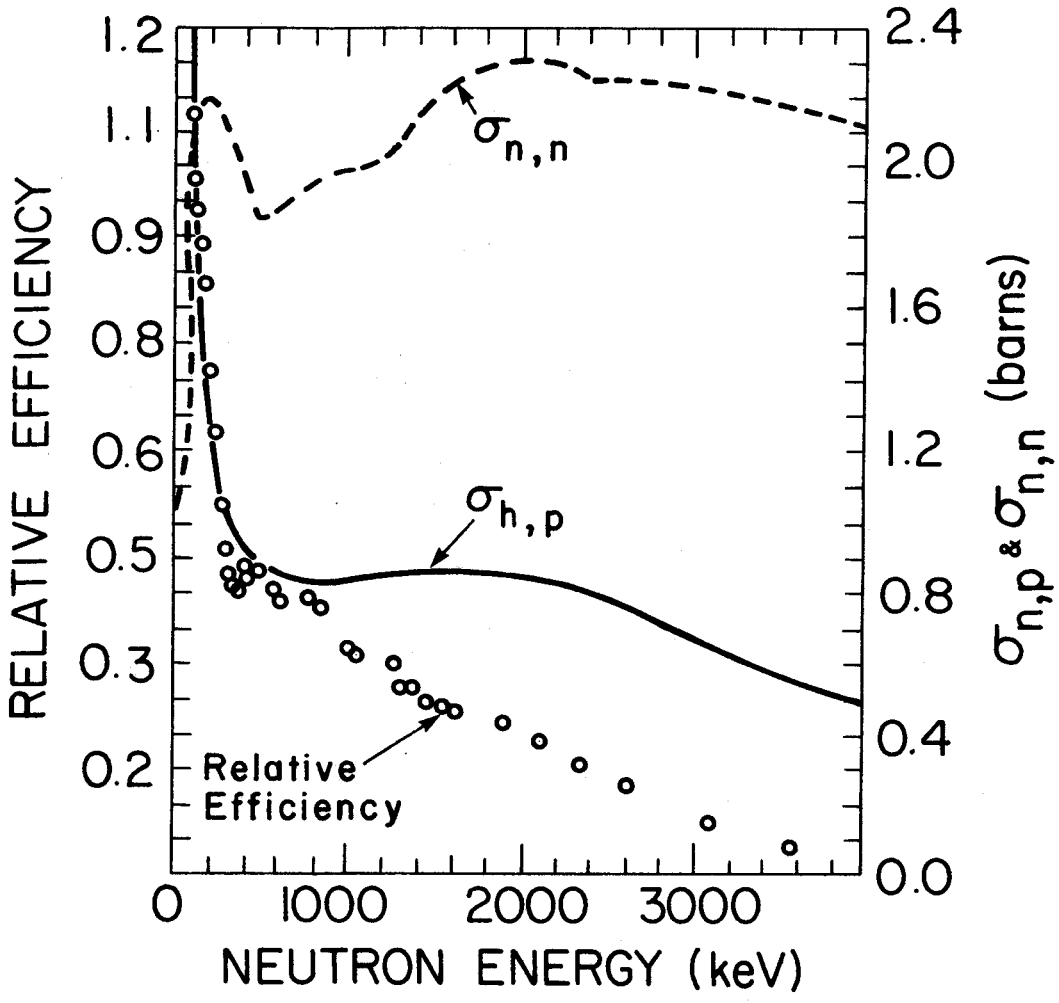
RELATIVE EFFICIENCY
1.2
1.1
0.9
0.8
0.6
0.5
0.3
0.2
2.4
2.0
1.6
1.2
0.8
0.4
0.0
$\sigma_{n,n}$
$\sigma_{h,p}$
Relative Efficiency
0
1000
2000
3000
NEUTRON ENERGY (keV)
$\sigma_{n,p}$ & $\sigma_{n,n}$ (barns)
PFC-8113

FIGURE 9

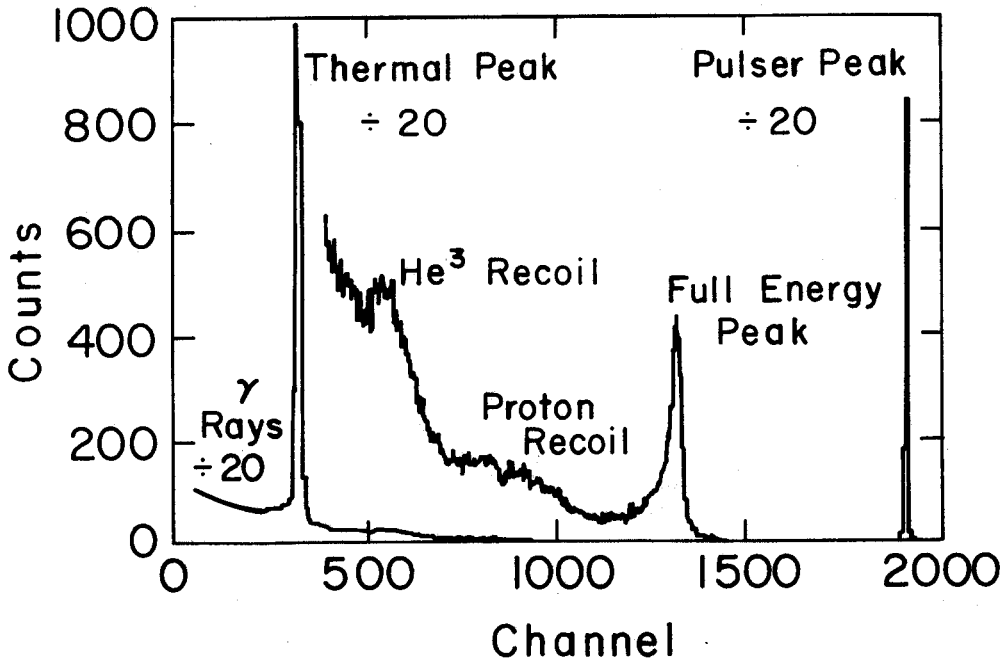

PFC - 8354

FIGURE 10

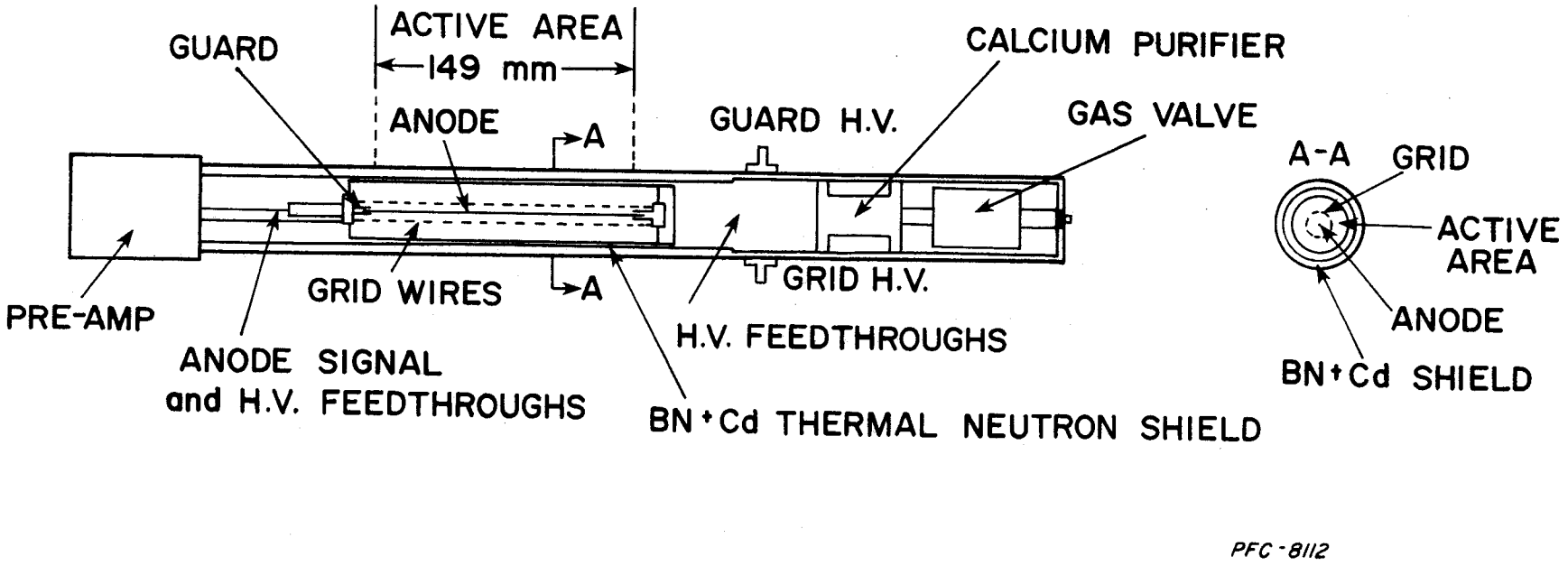
GUARD
ACTIVE AREA
149 mm
ANODE
A
GUARD H.V.
CALCIUM PURIFIER
GAS VALVE
A-A
GRID
ACTIVE AREA
ANODE
BN+Cd SHIELD
PRE-AMP
GRID WIRES
A
GRID H.V.
H.V. FEEDTHROUGHS
ANODE SIGNAL
and H.V. FEEDTHROUGHS
BN+Cd THERMAL NEUTRON SHIELD
PFC-8112

FIGURE 11

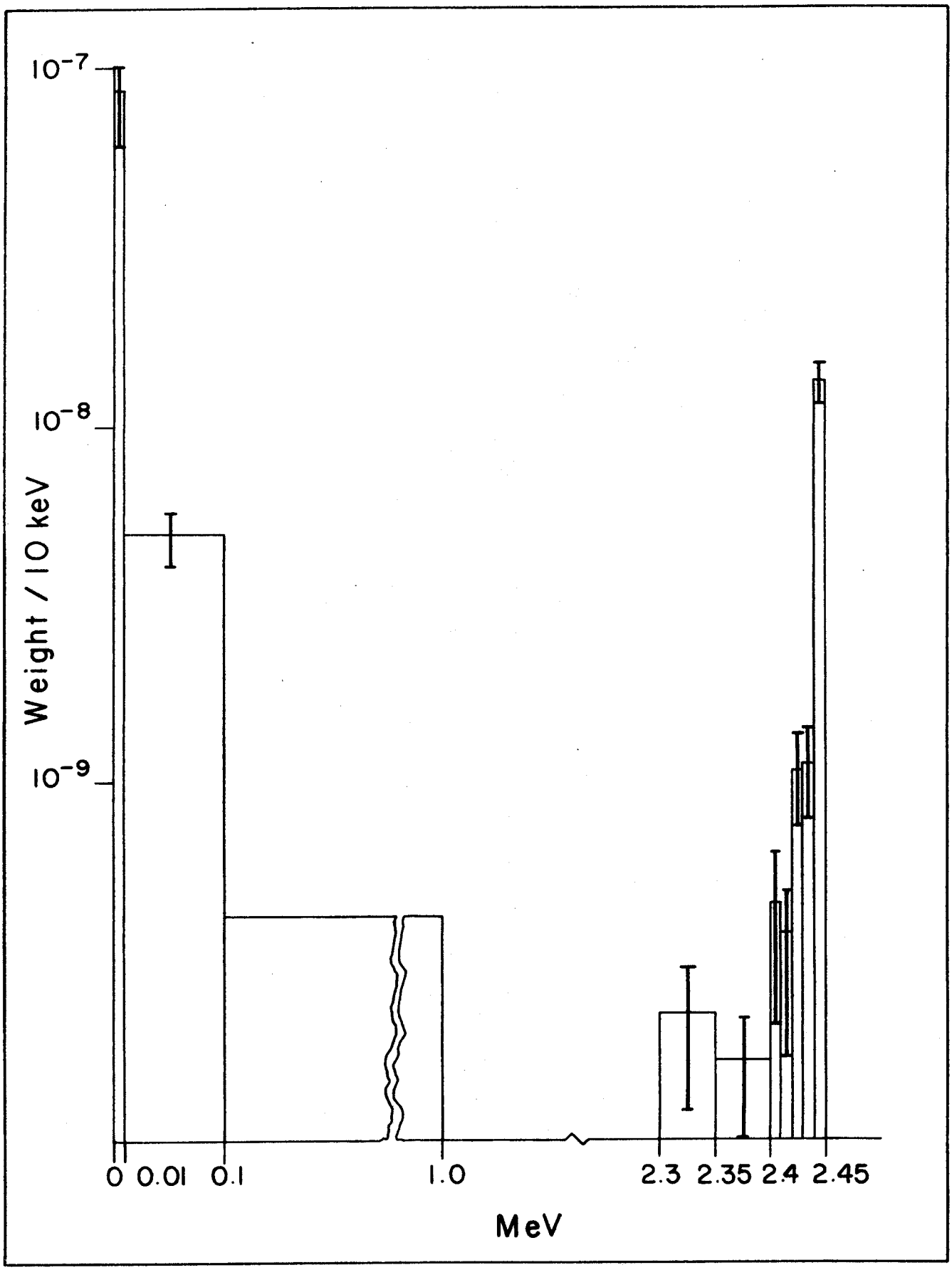

FIGURE 12

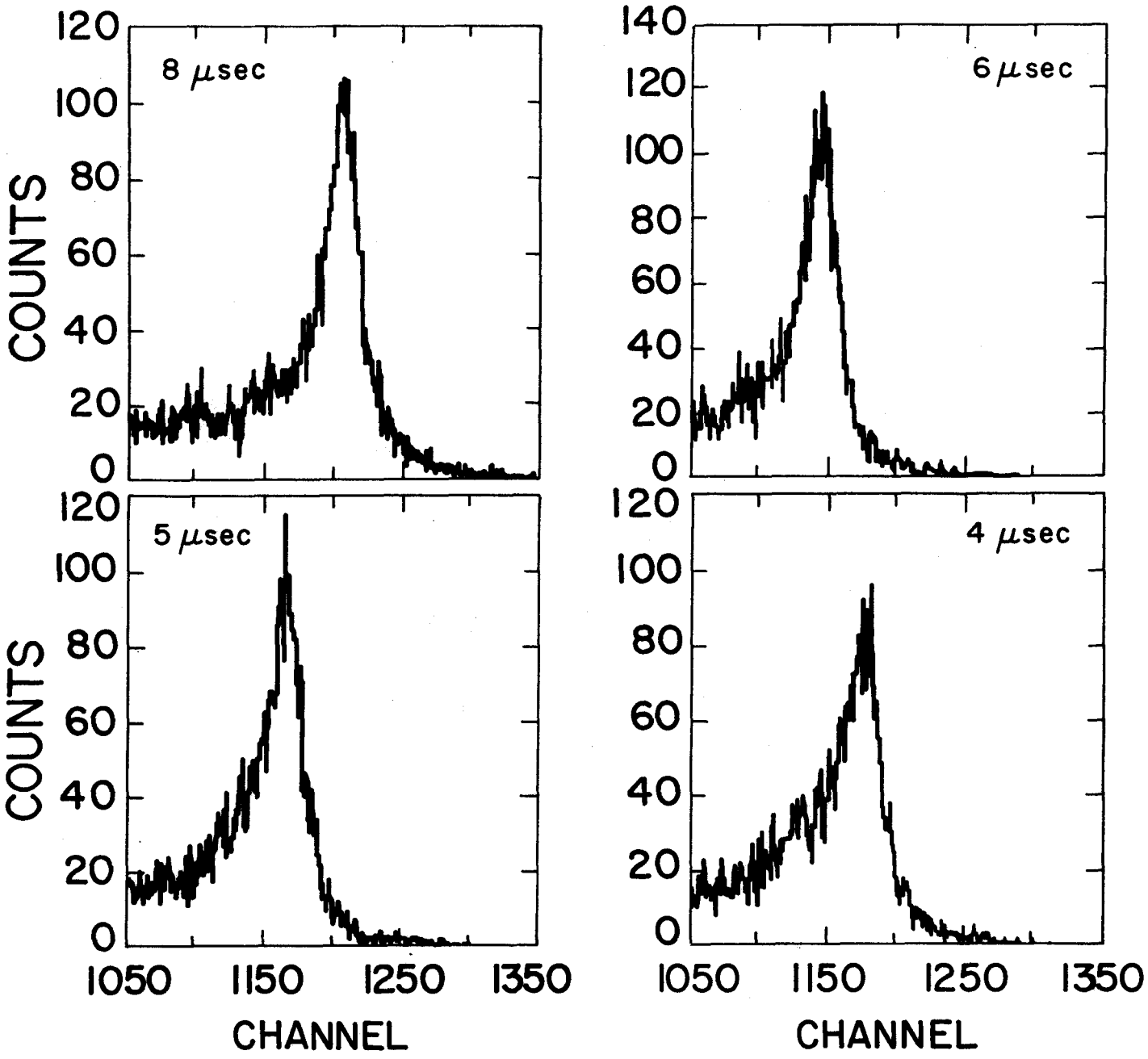
8 μsec
6 μsec
5 μsec
4 μsec
COUNTS
COUNTS
CHANNEL
CHANNEL
1050
1150
1250
1350
PFC-8122

FIGURE 13

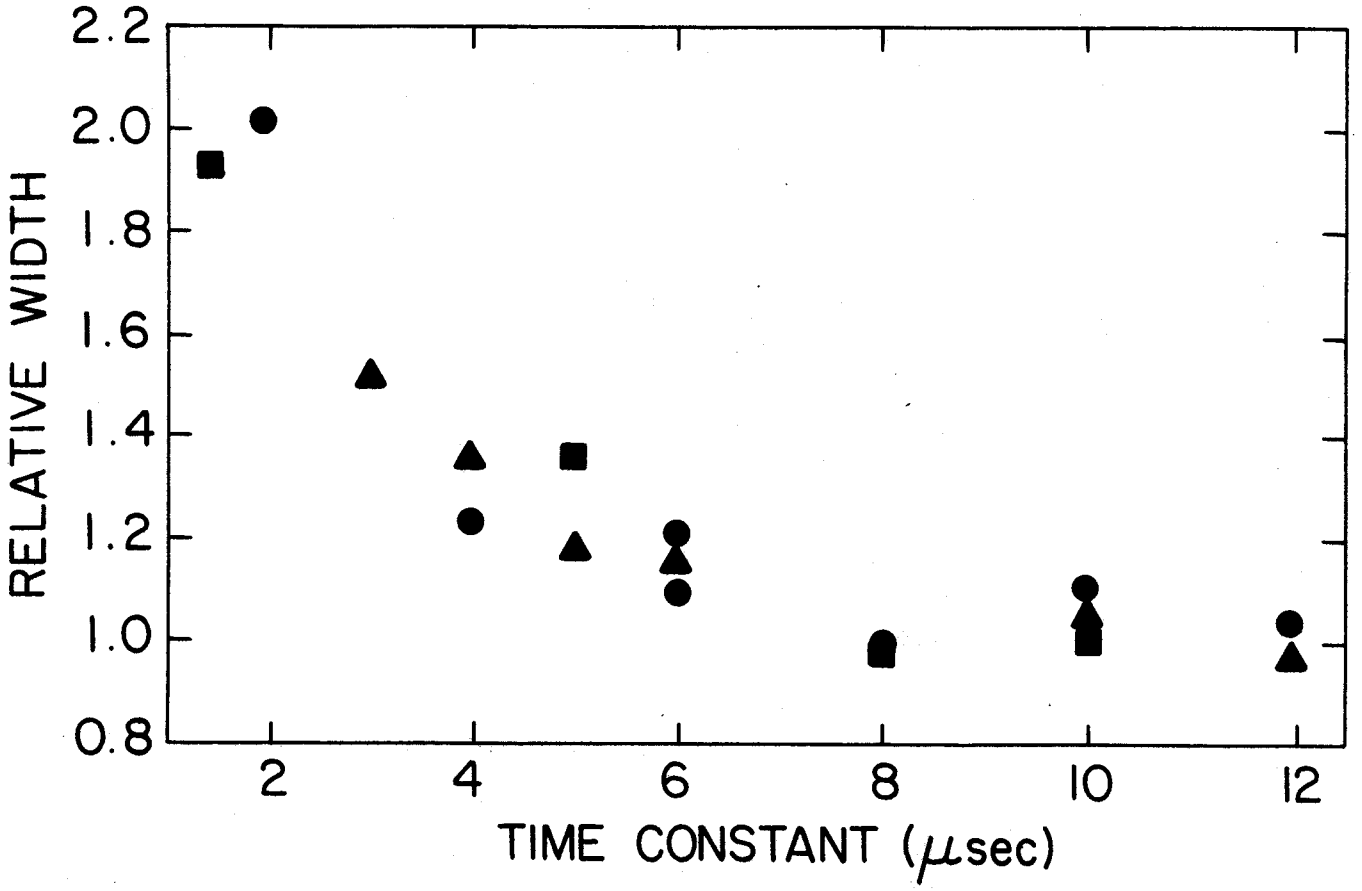
RELATIVE WIDTH
2.2
2.0
1.8
1.6
1.4
1.2
1.0
0.8
2
4
6
8
10
12
TIME CONSTANT (μsec)
PFC-8114

FIGURE 14

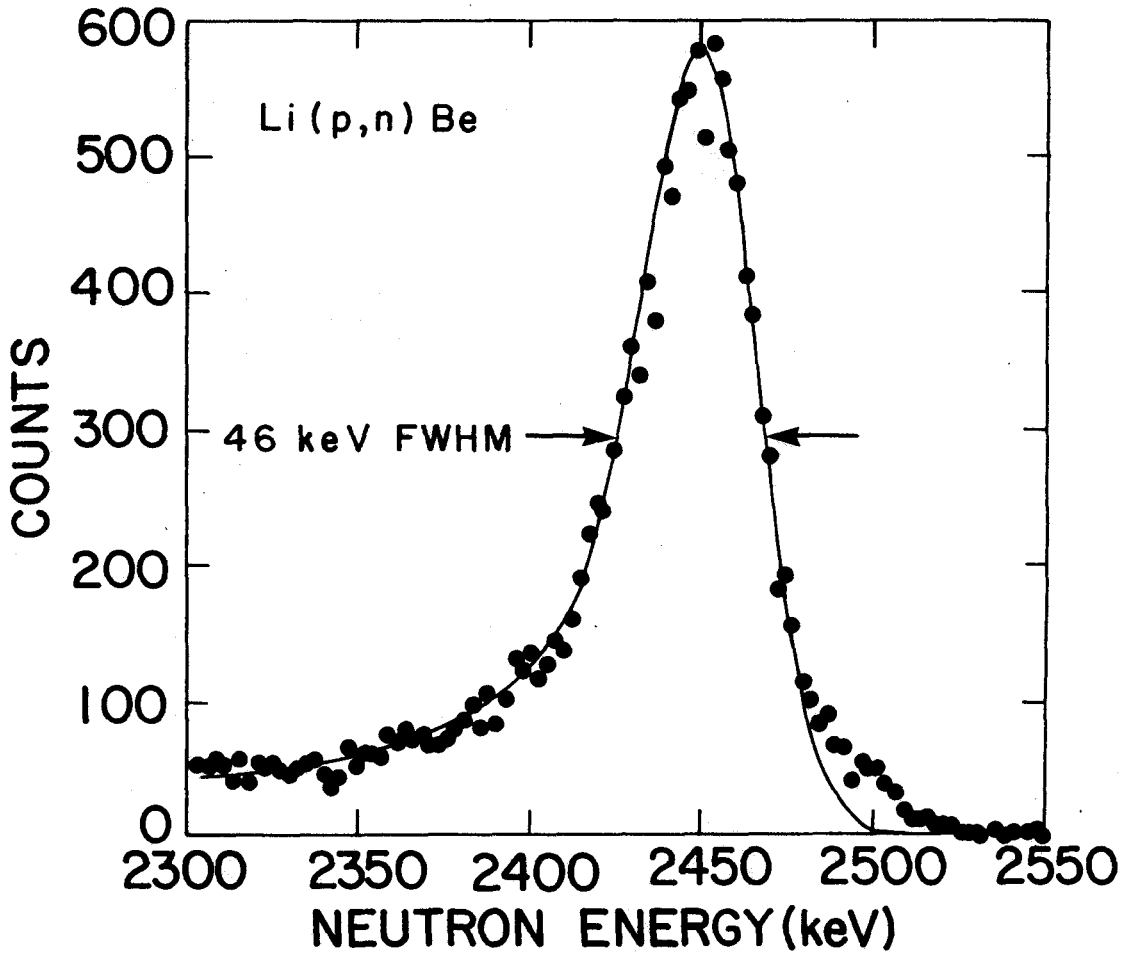
600
500
400
300
200
100
0
COUNTS
Li(p,n) Be
46 keV FWHM
2300
2350
2400
2450
2500
2550
NEUTRON ENERGY(keV)
PFC-8155

FIGURE 15

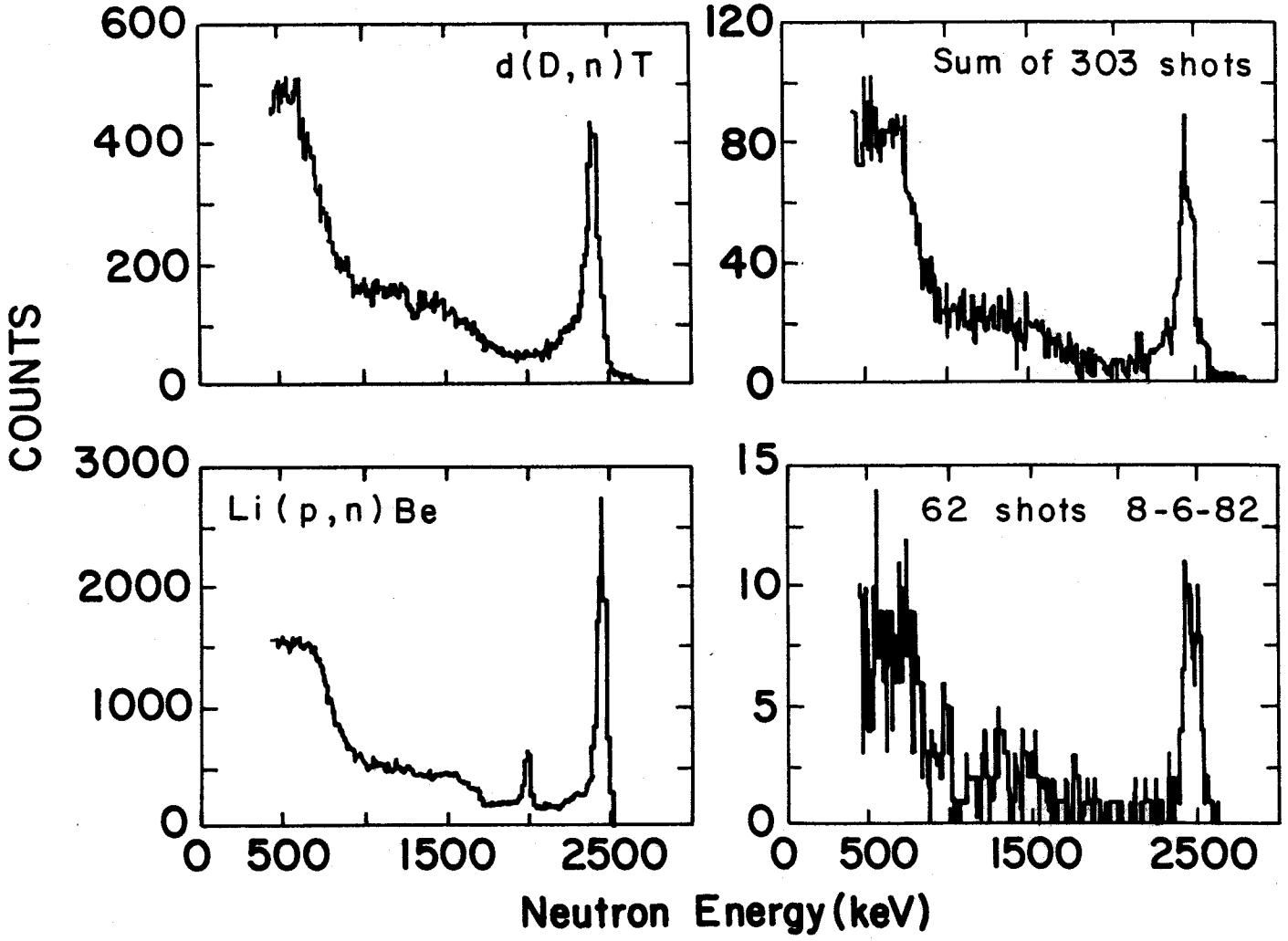

PFC-8120

FIGURE 16

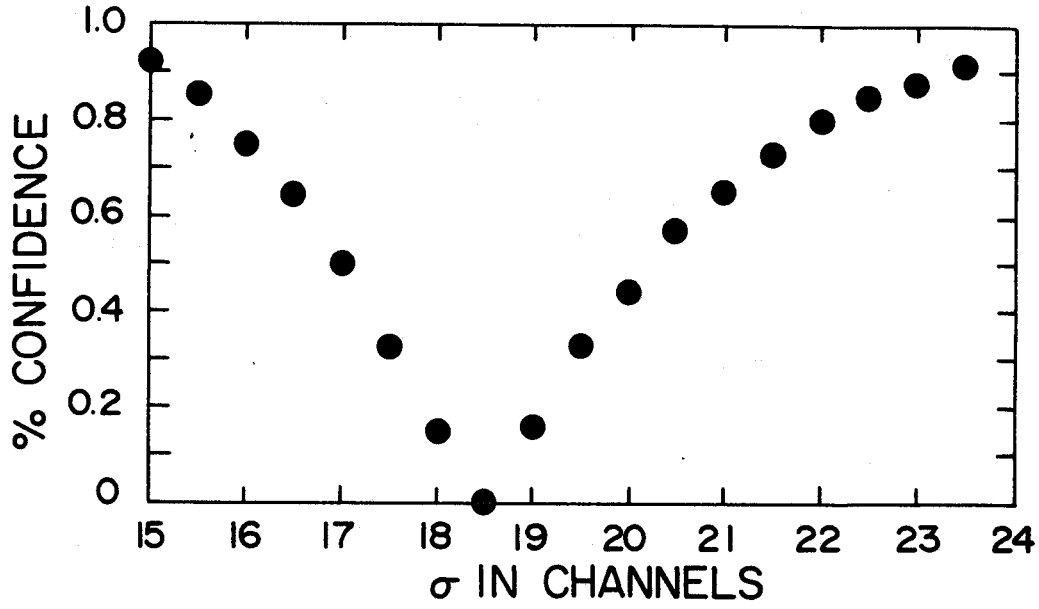
1.0
0.8
0.6
0.4
0.2
0
% CONFIDENCE
15
16
17
18
19
20
21
22
23
24
σ IN CHANNELS
PFC-8124

FIGURE 17

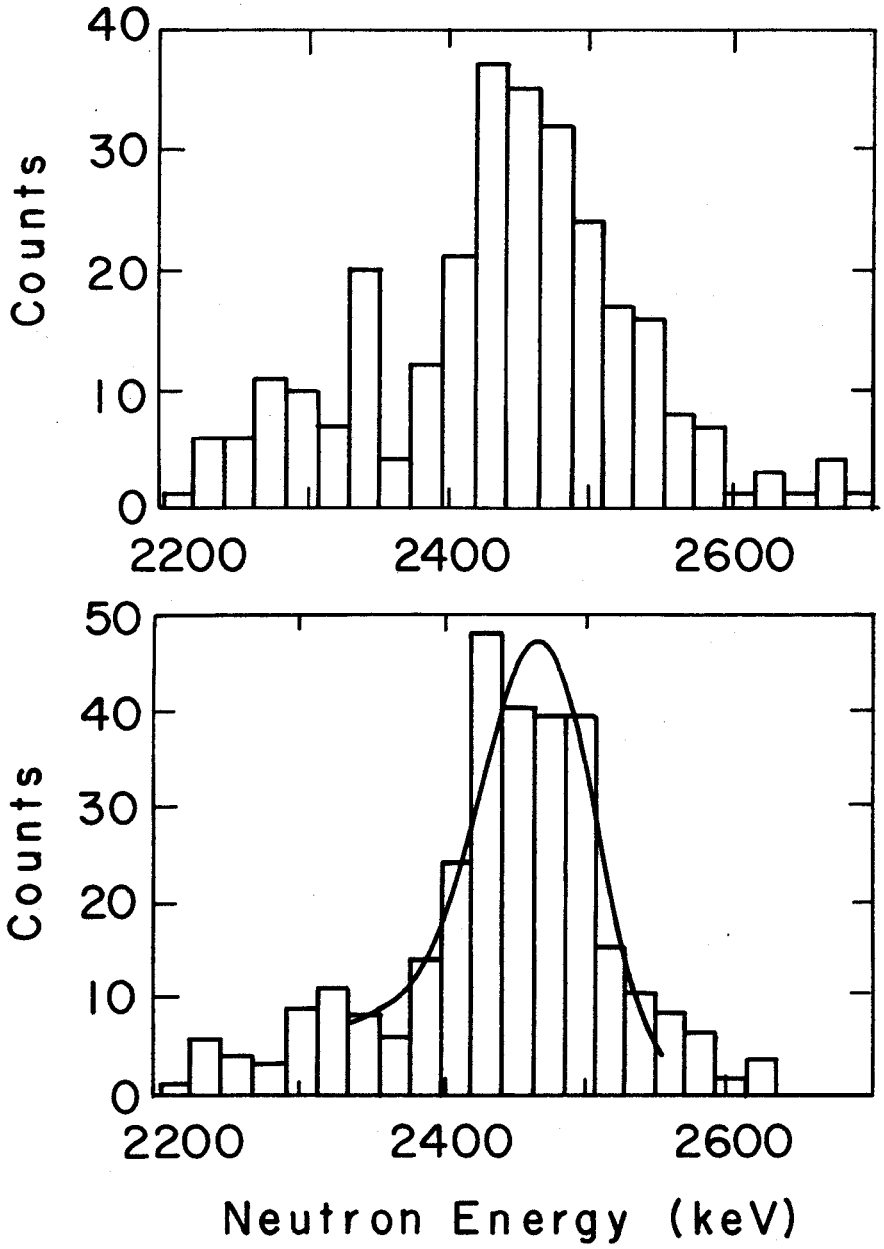

PFC - 8356

FIGURE 18

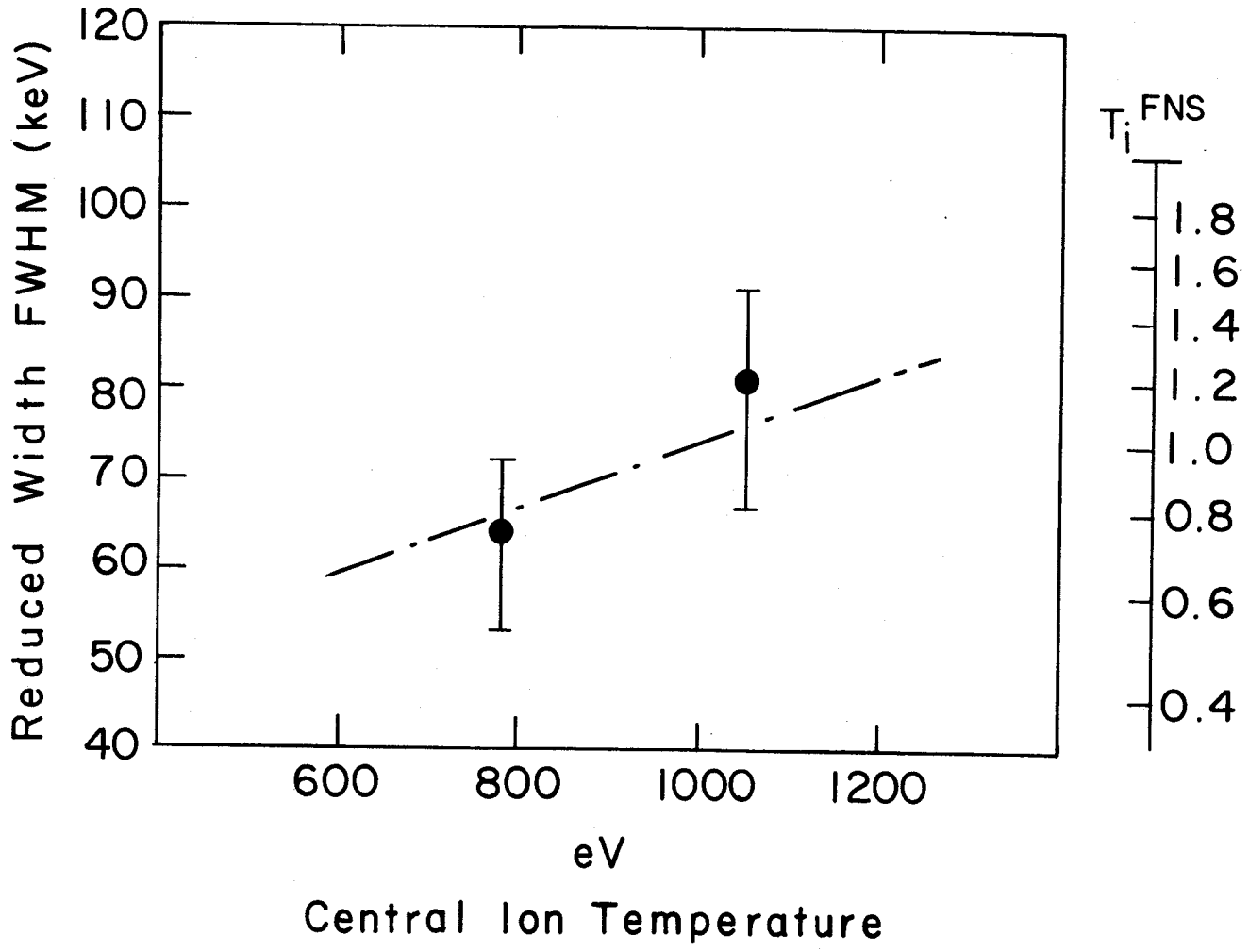

PFC-8357

FIGURE 19